

DATA-ENHANCED STOCHASTIC DYNAMICAL MODELING FOR WIND FARMS

by

Aditya H. Bhatt

APPROVED BY SUPERVISORY COMMITTEE:

---

Armin Zare, Chair

---

Mario A. Rotea

---

Stefano Leonardi

---

Jie Zhang

Copyright © 2022

Aditya H. Bhatt

All Rights Reserved

*To my parents and my brother*

DATA-ENHANCED STOCHASTIC DYNAMICAL MODELING FOR WIND FARMS

by

ADITYA H. BHATT, BE

THESIS

Presented to the Faculty of  
The University of Texas at Dallas  
in Partial Fulfillment  
of the Requirements  
for the Degree of

MASTER OF SCIENCE IN  
MECHANICAL ENGINEERING

THE UNIVERSITY OF TEXAS AT DALLAS

December 2022

## ACKNOWLEDGMENTS

I extend my sincerest gratitude to the numerous people who were instrumental in my graduate education and the successful composition of this thesis.

The first person I would like to thank is my advisor, Professor Armin Zare, for providing me the opportunity to explore an area of research in that I had very little prior experience. His hands-on approach, guidance and mentoring helped me push my boundaries and learn new subjects. His passion, dedication and commitment towards his work has been a great source of inspiration. Through his constant support, I have been able to overcome many challenges faced during my graduate studies.

I would like to thank Professors Rotea, Leonardi and Zhang for being willing to serve on the committee. Professor Leonardi and Federico Bernardoni have also been extremely generous in allowing access to simulation data for numerical experiments for this thesis.

One of the most cherished memory during my graduate studies was the chance to meet some wonderful labmates: Arya, the senior most member in the research group, who assisted me in learning the tools for the research; Mireille, who is working on extension of the this work; and the colleagues - Jonas, Vighnesh, Wenqing, Daniel, Dr. Benjamin Gravell, Sleiman who made this journey enjoyable.

My heartiest thanks goes to my family, who have imparted confidence in me by always believing in me. I will forever be indebted to my parents, Hitesh and Trupti, for their unconditional love, support and countless sacrifices to make sure that my brother and I receive the best education and achieve all our ambitions. To my brother, Bhavik, who made sure I am updated about things outside studies and do not miss out on life, I give my warmest gratitude. I would also like to thank my entire support system in the US: my aunts Nisha and Bhawini, my uncles Sunil, Alok and Karan and my sisters Hiya, Krisha and Siddhi for making me feel at home. Finally, a sincere thanks to the grandparents, aunts, uncles, cousins and all the family members back in India who have encouraged me over the years.

December 2022

# DATA-ENHANCED STOCHASTIC DYNAMICAL MODELING FOR WIND FARMS

Aditya H. Bhatt, MS  
The University of Texas at Dallas, 2022

Supervising Professor: Armin Zare, Chair

Low-fidelity analytical models of turbine wakes have traditionally been used to demonstrate the utility of advanced control algorithms in increasing the annual energy production of wind farms. In practice, however, it remains challenging to achieve significant performance improvements using closed-loop strategies that are based on conventional low-fidelity models. This is due to the over-simplified static nature of wake predictions from models that are agnostic to the complex aerodynamic interactions among turbines. In this thesis, we offer a stochastic dynamical modeling framework to improve the predictive capability of low-fidelity models while remaining amenable to control design. The framework is capable of capturing the effect of atmospheric turbulence on the thrust force and power generation as determined by the actuator disk concept. In this approach, we use stochastically forced linear models of the turbulent velocity field to augment the analytically computed wake velocity and achieve consistency with higher-fidelity models in capturing power and thrust force measurements. The power-spectral densities of our stochastic models are identified via convex optimization to ensure statistical consistency while preserving model parsimony. We demonstrate the utility of our approach in estimating the thrust force and power signals generated by large-eddy simulations of the flow over a cascade of turbines. We also evaluate the capability of our models in predicting turbulence intensities at the hub height of a multi-turbine wind farm.

## TABLE OF CONTENTS

ACKNOWLEDGMENTS . . . . .	v
ABSTRACT . . . . .	vi
LIST OF FIGURES . . . . .	ix
CHAPTER 1 INTRODUCTION . . . . .	1
1.1 Wind farm control . . . . .	3
1.2 Stochastic dynamical modeling of turbulent flows . . . . .	7
1.3 Organization of the thesis . . . . .	8
CHAPTER 2 ENGINEERING WAKE MODELS . . . . .	10
2.1 Wake modeling based on co-flowing jets . . . . .	11
2.2 Park Model . . . . .	12
2.3 Eddy viscosity model . . . . .	12
2.4 Gaussian deficit model . . . . .	14
2.5 Wake superposition . . . . .	14
2.6 Shortcomings of the analytical wake models . . . . .	15
CHAPTER 3 STOCHASTICALLY FORCED LINEARIZED NAVIER-STOKES . .	18
3.1 Linearized Navier-Stokes . . . . .	19
3.2 Volume penalization technique . . . . .	21
3.3 Second-order statistics of LTI systems . . . . .	22
CHAPTER 4 STOCHASTICAL DYNAMICAL MODELING OF PARTIALLY AVAIL- ABLE STATISTICS . . . . .	25
4.1 Covariance completion . . . . .	26
4.2 Stochastic realization . . . . .	27
CHAPTER 5 STOCHASTIC DYNAMICAL MODEL FOR WIND FARMS . . . . .	29
5.1 Large-eddy simulations . . . . .	29
5.2 Base flow . . . . .	30
5.3 System matrices in linearized NS equations in evolution form and boundary conditions . . . . .	31
5.4 Thrust force and power predictions . . . . .	32

5.5	Turbulence intensity predictions . . . . .	34
5.6	Verification in stochastic linear simulations . . . . .	38
CHAPTER 6 CONCLUSIONS AND FUTURE DIRECTIONS . . . . .		40
6.1	Conclusions . . . . .	40
6.2	Future Directions . . . . .	41
REFERENCES . . . . .		42
BIOGRAPHICAL SKETCH . . . . .		51
CURRICULUM VITAE		



## LIST OF FIGURES

1.1	(a) Global energy consumption by source based on the substitution method which takes into account the inefficiencies of the fossil fuel production [40],(b) The total energy consumption in the US based on the source of generation (source: <a href="#">EIA</a> ).	2
1.2	Interactions between the turbulent ABL and wind farms through turbulent eddies and meandering streamwise streaks of high- and low-speed winds. . . . .	4
1.3	Parsimonious modifications of linearized dynamics are formed via the cascade connection of the linearized dynamics with a spatio-temporal filter that is designed to account for available output statistics. . . . .	8
2.1	The actuator disk model (ADM). The rotor is considered as a porous disk that extracts the kinetic energy from the wind while reducing the wind velocity [14].	11
2.2	Schematic representing the top-hat approach for modeling the wake. The turbine is represented with thick black line and the uniformly growing wake profile is shown about the center line (dashed) . . . . .	13
2.3	The normalized wake velocity using the Gaussian profile for the deficit calculated using Eq. 2.1. The turbine is indicated with the thick black line. . . . .	15
2.4	Geometric sketch of a 2D grid of collocation points around a turbine rotor. The sample grid demonstrates the division of the turbine rotor into 3 equally sized segments. The staggered points where the effective velocities $\mathbf{u}_{\text{eff}}$ and the intensities used in Equations (3.2) are computed are marked by the red dots. . . . .	16
2.5	(a) Predictions of thrust force $\bar{F}$ and (b) power generation $\bar{P}$ from LES (*) and the result of using Equation (2.4) with 15 segments across the spanwise extent of turbine rotors (see Fig. 2.4) and the velocity field predicted by the analytical model (5.2) (●). . . . .	16
3.1	(a) A cascade of 4 equally spaced turbines. (b) The streamwise and spanwise dependence of the velocity field $\bar{\mathbf{u}}(x, z)$ generated by the analytical model (5.2) from Bastankhah and Porté-Agel [8] over the 2D computational domain at hub height. The thick black lines mark the location of the turbine rotors. . . . .	20
3.2	(a) The spanwise dependence of the resistance function $K^{-1}(z)$ following Equation (3.6) with $z_1 = -0.1$ , $z_2 = 0.1$ , $a = 5$ , and $c = 400$ . (b) The streamwise and spanwise dependence of the resistance function $K^{-1}(x, z)$ corresponding to Equation (3.6). . . . .	22
3.3	The eigen spectrum analysis of the dynamic generator $A$ with tuneable parameter (a) $c = 0$ , (b) $c = 50$ , (c) $c = 100$ , (d) $c = 150$ , (e) $c = 184$ , (f) $c = 185$ in the resistance function Eq. 3.6. (*) are stable eigen values and (*) denoting the unstable eigen values. . . . .	23

5.1	(a) Results for matching thrust force $\bar{F}$ and predicting power generation $\bar{P}$ over various turbines in the $4 \times 1$ cascade; (b) Results for matching power generation $\bar{P}$ and predicting thrust force $\bar{F}$ ; (c) Results for matching the balanced approximation of both thrust force and power. LES data (*); predictions of analytical model [8] (●); and predictions of our data-enhanced stochastic dynamical model (○). . . . .	34
5.2	(a) Schematic of hub-height computational plane with data points used for training in Section 5.5.1 highlighted in red; (b) Hub-height streamwise velocity $\bar{\mathbf{u}}(x, z)$ generated using the analytical wake-expansion model of Bastankhah and Porté-Agel [8] around which we linearize the NS equations. . . . .	35
5.3	(a) Streamwise turbulence intensity ( $uu$ ) obtained from LES and (c,e,g) the results of our stochastic dynamical model with data provided at $1d_0$ (c), $2d_0$ (e), and $3d_0$ (g) locations downstream of the turbine as shown by the blue dots in the figures on the left. . . . .	36
5.4	(a) Spanwise turbulence intensity ( $ww$ ) obtained from LES and (c,e,g) the results of our stochastic dynamical model with data provided at $1d_0$ (c), $2d_0$ (e), and $3d_0$ (g) locations downstream of the turbine as shown by the blue dots in the figures on the left. . . . .	37
5.5	Streamwise $uu$ (left) and spanwise $ww$ (right) turbulence intensities resulting from LES (a,b) and our stochastic dynamical models (c,d) trained using all intermediate locations downstream of the turbine nacelle and blade tips shown by the blue dots in the plots on the last row. . . . .	39
5.6	Time evolution of fluctuation kinetic energy for 20 realizations of the forcing to the modified linearized dynamics; the energy averaged over all simulations is marked by the thick black line. . . . .	39
6.1	Our proposed modeling approach which uses data to augment the low-fidelity model using a stochastic dynamical representation thus, providing improvements to their predictive capabilities. . . . .	41

# CHAPTER 1

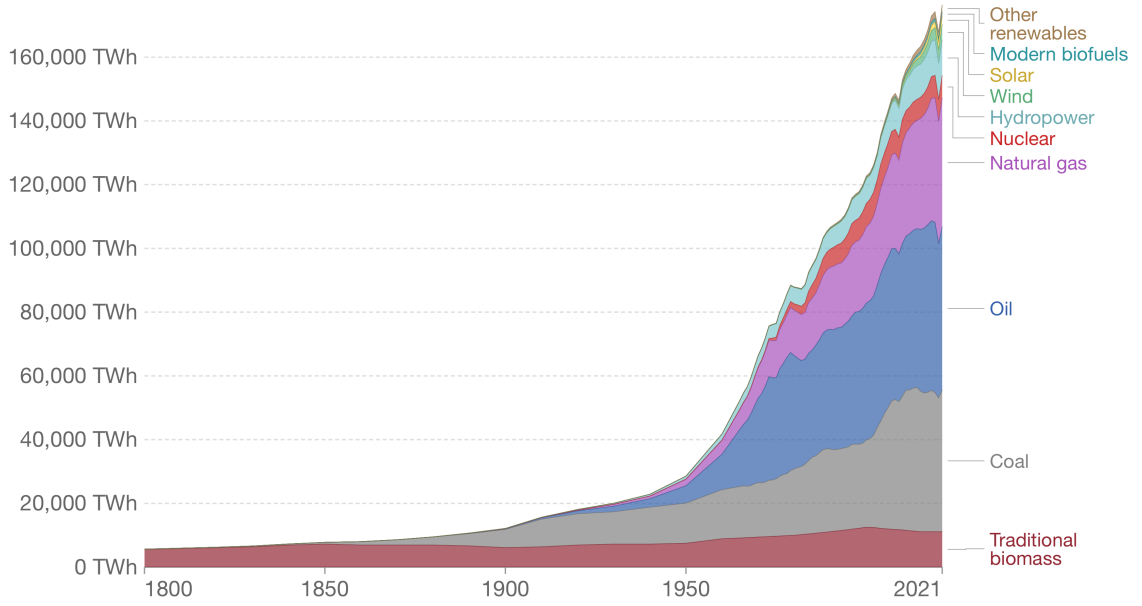
## INTRODUCTION

The constantly evolving technological landscape is evident with the presence of smart devices in our day-to-day lives. While the intended use of such devices is to improve our lifestyle, a consequence is the increasing energy consumption and subsequently escalating demands on the global energy production. The UN world population prospects estimate a global population of approximately 10 billion by 2050 [104]. Moreover, based on the projection by US Energy Information Administration (EIA), the global energy demand is expected to reach 45 trillion KWh per year in 2050 up from 25 trillion KWh in 2022. Traditionally, the energy industry has mainly relied on the use of fossil fuels, oil or harvesting the heat generation through nuclear fission as primary sources for producing electric power. However, not only are fossil fuels non-renewable resources, their energy extraction process comes with carbon footprint. Moreover, assuring stability of operation and safe disposal of cooling agents in a nuclear power plant is an arduous task. A growing realisation of the shortcomings and environmental hazards associated with these methods has led to a shift in emphasis towards utilisation of sustainable energy resources such as solar and wind. Advancements in material science have enabled development of solar panels that are small and light in weight, thus enabling use beyond the commercial sector. Further, thanks to the contributions of Albert Betz and others during start of 20<sup>th</sup> century, the foundations of wind energy science were laid. This led to the use of wind turbines, which were often used as mills in farms, as dynamos for producing electricity.

The installed capacity of solar and wind energy has been growing exponentially with a forecasted 4800 GW global capacity by 2026. In spite of such high numbers, renewable energy contributes to a mere 12% of energy consumption in the US (see Figure 1.1(b)). One of the reasons for these low numbers is efficiency. While solar energy is roughly 23% efficient, wind energy conversion is close to 50% efficient [107]. Such low outputs impact the cost of energy extraction thus making it an unfavourable prospect not only for companies but also for end users. In order to meet at least a half to two-third of the global energy demands while maintaining economical viability, there needs to be a strategic plan for advancement of knowledge and transfer of modern technologies to the industry.

The levelized cost of energy (LCOE) for wind farms is obtained as a ratio of the total energy production to the total investment in installation and maintenance of the farm throughout its life cycle (approx. 20 years). Thus, in order to produce energy in a cost

(a)



(b)

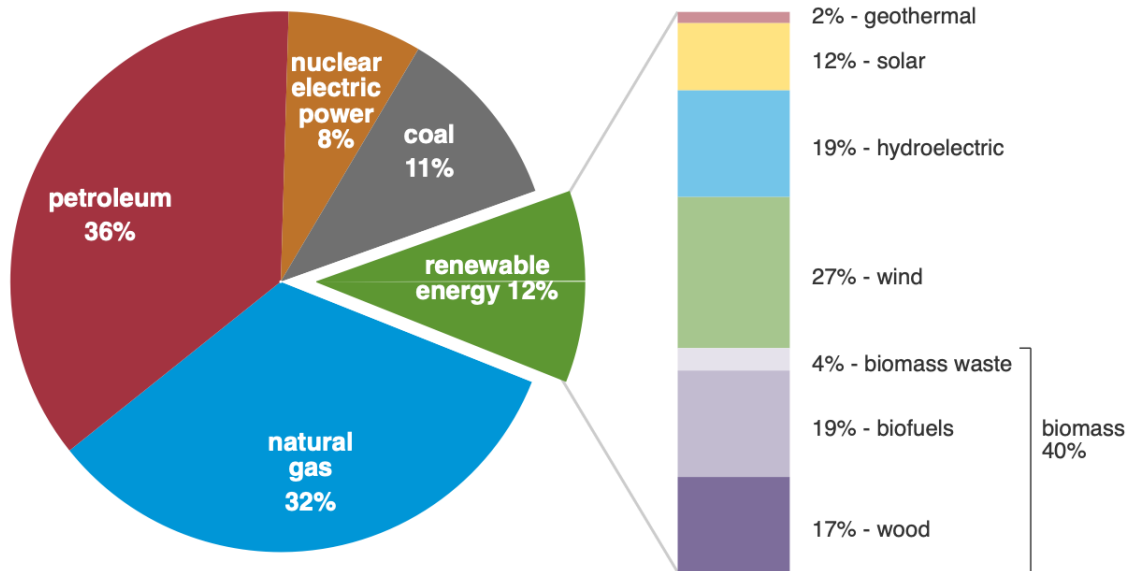


Figure 1.1: (a) Global energy consumption by source based on the substitution method which takes into account the inefficiencies of the fossil fuel production [40],(b) The total energy consumption in the US based on the source of generation (source: [EIA](#)).

effective manner, focus needs to be centered around increasing the efficiency and ensuring durability of mechanical and structural components. In [106], the authors have highlighted these aspects and captured the key challenges in the science of wind energy, namely: (i) improved understanding of physics of atmospheric flow in the critical zone of wind power plant operation, (ii) material and system dynamics of individual turbines, and (iii) optimization and control of fleets of wind plants comprising hundreds of individual generators working synergistically within the larger electric grid systems. Given the fact that these challenges are interlinked and multidisciplinary, overcoming them can not be achieved in isolation rather a coordinated development of all aspects related to wind turbine technology is required.

The first challenge relates to region of operation of the wind turbines in earth's atmosphere. Wind turbines operate in the atmospheric boundary layer (ABL), which exists in the intermediary region between the ground and the geostrophic wind above and is canonically composed of a mean shear flow and fluctuations that span a wide range of scales [100]. The diverse range of coherent motions in the ABL affect the development of wakes behind turbines and thereby energy production and structural durability within wind farms [77, 99]. For example, dominant streamwise elongated streaks of high-and low-speed winds at the wind farm scale and mesoscale have been linked to turbine wake meandering in the lateral directions (Figure 1.2) [77, 99]. However, ABL conditions have a decreasing relevance as wind penetrates deeper into an array of turbines within a farm. Instead, downstream turbine wakes are impacted by the wakes of upstream ones and vertical kinetic energy entrainment from high speed flows above hub height. Through such nonlinear interactions, turbine wakes reduce the incoming ABL's mean streamwise velocity while increasing turbulence intensity [7, 99], which defines the second challenge of ensuring structural rigidity of the turbines. The effective entrainment of kinetic energy and turbine-induced mixing results in a reduction in power production and an elevation in dynamic loads. A possible way to overcome such negative effects can be achieved through the coordination and control of turbines.

## 1.1 Wind farm control

Wind streams are caused due to the earth's rotation, coriolis forces, and uneven heating of the surface. The key characteristics of wind are its speed and direction of flow. Given the dependence of wind characteristics on factors such as geography and terrain, wind speed and direction at a specific location are not constant. The changes in these quantities can

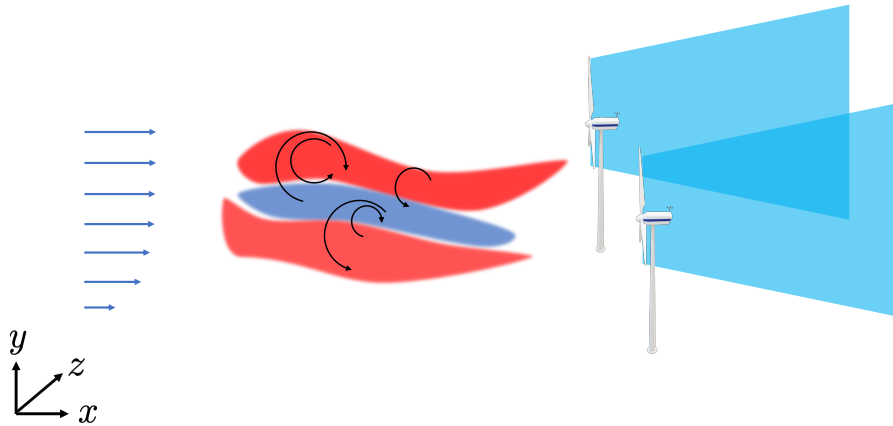


Figure 1.2: Interactions between the turbulent ABL and wind farms through turbulent eddies and meandering streamwise streaks of high- and low-speed winds.

occur over a day (i.e diurnal) or longer period of time. Wind turbines would ideally function the best while facing the wind at all times and operating under a steady velocity. However in reality, wind turbines need to be yawed to face the wind and a gearbox is required to assist with variable speeds of operation. To perform these tasks in a scientific manner, researchers have suggested the use of control strategies that can enhance the collective performance of wind turbines located with close proximity (i.e. wind farms). In recent years, many simulation-based and experimental studies have demonstrated the efficacy of induction and wake steering as control strategies that can improve the performance of wind farms [2, 12, 24, 27, 30, 31, 42, 94]. To date, most studies have focused on open-loop control policies that are informed by look-up tables that determine the optimal turbine settings offline and based on the response of static engineering models to different steady-state atmospheric conditions, i.e., wind directions, wind speed, turbulence intensity, etc. Model-free methods, e.g., extremum seeking control, have also been proposed for maximizing power production [19, 21, 49]. While such open-loop approaches are shown to be successful in controlled numerical or experimental testing environments [12, 19, 31, 42], potentially unforeseen variations in turbulent inflow conditions, terrain specific effects, or sensing/actuation errors can hinder their generalizability, and thus, their applicability at the scale of large wind farms. Robust feedback control provides the systematic means to tackle such challenges by account-

ing for uncertainties in sensing and actuation, unknown exogenous disturbances, in addition to modelling errors [97, 118].

The vast range of scales over which coherent structures affect turbine performance coupled with the interplay between scales, in addition to the complexities of wake turbulence necessitate the development of control-oriented models for the analysis and control of wind farms [105, 106]. Nevertheless, closed-loop control design has predominantly relied on computationally expensive high-fidelity models such as those that are used in large-eddy simulations (LES) to demonstrate meaningful performance improvements [25, 26, 36, 37, 70, 71, 72, 95]. While such models play an important role in improving our understanding of wake turbulence, they are not suitable for the development of online model-based control strategies that can adapt to time-varying atmospheric conditions informed by supervisory control and data acquisition (SCADA) measurements. This motivates the development of lower fidelity models that capture the essential flow features and quantities of interest for analysis or control.

Seminal efforts in developing low-fidelity models of turbine wakes focused on two-dimensional (2D) heuristic based methods that capture the reduction in the mean streamwise velocity at hub height for given steady atmospheric conditions [3, 48, 57]. Enabled by structural approximation of turbine rotors, e.g., the actuator disk model (ADM) [14], more sophisticated variants that observe conservation principles for mass and momentum [32] or even model the mean streamwise velocity deficit as a Gaussian distribution [8] were combined with linear wake superposition laws to provide more reasonable predictions of the power captured by wind farms. The predictions of such static engineering models of the averaged velocity field typically depend on a set of parameters that can be tuned to match field measurements or LES data, e.g., [16, 109, 117]. Efforts have also been made to incorporate 3D effects resulting from turbine yawing or ground effects into numerical integration schemes and predict the curled shape of turbine wakes [65, 66, 119]. More recent analytical developments bypass the need for numerical integration while accounting for curled shape deformations and even lateral and wall-normal deflections of turbine wakes due to, e.g., the ground [9]. Nevertheless, in the absence of a dynamical model for background turbulence, the over-simplified static nature of conventional engineering wake models that neglects the time-varying features of near-field turbulence leads to the under-prediction of wake recovery. This, in turn, can yield inaccurate predictions of quantities of interest for wind farm control, i.e., the load and power corresponding to each turbine.

To overcome the shortcomings of static engineering models, contributions have been made to add a degree of dynamics or parametric stochasticity to analytical models, e.g.,

the dynamic wake-meandering model [60], models that incorporate time-delays to capture wakes that travel at free-stream velocity [33], the dynamic extension of the Park model [4], and the stochastic ADM model [39]. Reliance on extensive parametric tuning, dynamical complexities, and the absence of constructive methods for uncertainty modeling challenge the utility of such models for real-time estimation and control. Medium-fidelity models, e.g., those that are based on the Reynolds-averaged NS (RANS) equations, have sought to overcome some of these issues by capture the 3D dynamic variation of the velocity field and introduce turbulence models that enable wake recovery [45, 10, 62]. The limitations of current turbulence models and the nonlinear nature of RANS-based models, however, hinder the utility of such models for optimal estimation and control strategies using conventional algorithms.

Machine learning approaches have also been used to obtain reduced-order models based on data collected from experiments and numerical simulations [47, 84, 96, 108]. Data-driven methods are attractive due to their flexibility in analyzing different physical phenomena. However, their utility in solving real-world problems is often challenged by the uninterpretability of dynamic links that are identified through optimization procedures, intricate multi-layer nature models that are identified via (deep) neural networks, and the reliance on extensive parametric tuning. Moreover, a detachment from the mathematics that govern the complex interaction between the ABL and turbine wakes can cause anomalies and insufficiencies in the training dataset to challenge the viability of purely data-driven methods in providing a robust, generalizable solution for real-time model-based estimation and control [74, 101].

In [98], the linearized Navier-Stokes (NS) equations were combined with vortex cylinder theory to provide a physics-based alternative for dynamical modeling of wind farm flows. Furthermore, in conjunction with actuator disk theory, the 2D linearized NS equation have been reformulated as a quasi linear parameter varying descriptor model and used for the purpose of wind farm control [11]. Linearized models can overcome some of the shortcomings of conventionally used low-fidelity wake models in qualitatively predicting flow features of turbulent wakes and the resulting power production [10]. However, quantifying and modeling the uncertainty due to (i) the choice of base flow around which we linearize the governing equations, and (ii) the absence of nonlinear terms remains challenging. Modeling such sources of uncertainty plays an important role in obtaining well-posed estimation gains [17, 41] when using linear models for predicting flow statistics or quantities of interest for control design, e.g., thrust force or power generation at turbines.



## 1.2 Stochastic dynamical modeling of turbulent flows

In this thesis, we propose to build on the stochastic dynamical modeling framework of [111, 112, 115, 116] to address the aforementioned challenges in the control-oriented modeling of wind turbine wakes. Our framework utilizes a data driven approach for enhancing the predictions of an underlying physics based model. The enhancement in predictions is obtained by subjecting a linear model to additive stochastic forcing that is shaped using statistics from the non-linear flow. In the presence of additive sources of deterministic or stochastic excitation, the linearized NS equations have been shown to capture structural and statistical features of transitional [15, 103, 28, 6, 53, 55, 79] and turbulent [67, 44, 115, 112] wall-bounded shear flows, in addition to facilitating model-based analysis and design of flow control strategies [54, 68, 69, 80]. Additive stochastic excitation provides a statistical response and allows for a qualitative and quantitative comparison between the predictions of the linear model and a turbulent flow field in terms of statistical quantities, e.g., the mean and variance of the velocity field. Such sources of excitation also capture the effect of the neglected nonlinearity as well as exogenous disturbances. Based on this, inverse problems can be posed to utilize statistical signatures of turbulent flows that are generated by numerical simulations of the NS equations (e.g., from [22, 23, 92, 93]) or experimental measurements (e.g., from [43, 91]) to shape the statistics of stochastic forcing. This approach to turbulence modeling was originally proposed by Zare and collaborators in [114, 111, 116], where a stochastic modeling framework was developed to account for partially observed statistical signatures of complex dynamical systems (e.g., turbulent flows) by introducing parsimonious perturbations to the linearized dynamics. Such dynamical perturbations are obtained using a systematic procedure for the realization of colored-in-time stochastic forcing of the linearized equations such that its output is statistically consistent with nonlinear simulations of the governing partial differential equations. The cascade connection of the linearized dynamics and the proposed filter dynamics that generate the stochastic forcing introduces a dynamical perturbation that acts as a data-driven enhancement to the linearized equations; see Figure 1.3.

Application of this framework to turbulent channel flows at different Reynolds numbers has demonstrated the efficacy of this approach in capturing various structural and statistical flow features. For example, when trained with one-point correlations of the velocity field (normal/shear stresses), it has been shown that such models not only perfectly *match* the one-dimensional energy spectrum, but they also reasonably *predict* two-point velocity correlations that are pertinent to the prediction of turbulent flow structures as well as spatio-temporal features, such as the power spectral density. The linear dynamics resulting from the cascade

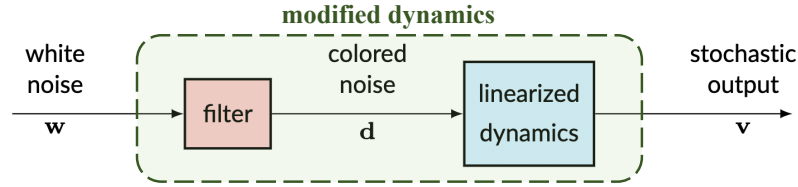


Figure 1.3: Parsimonious modifications of linearized dynamics are formed via the cascade connection of the linearized dynamics with a spatio-temporal filter that is designed to account for available output statistics.

connection shown in Figure 1.3 can be analyzed using tools from systems theory and used to generate turbulent flow statistics via inexpensive stochastic linear simulations; see [115, 112] for details. In this thesis, we build on the stochastic dynamical modeling framework of [111, 115, 112, 116] to augment the predictions of low-fidelity analytical models with the fluctuating velocity field obtained via stochastically forced linear models that are trained to match SCADA measurements or LES-generated data.

### 1.3 Organization of the thesis

The remainder of this thesis is organised into five chapters and an appendix. In summary, the thesis explains the stochastic dynamical modeling framework applied to a wind farm.

- Chapter 2 explains the actuator disk model for wind turbine which is the basis for different analytical wake models existing in the literature. The models apply basic laws of conservation of mass and momentum to compute the wind velocity profile. We also highlight the shortcomings of these models in predicting the key quantities such as the thrust force and power in a wind farm.
- Chapter 3 provides an augmentation to the analytical relationships for thrust force and power in order to improve the predictions of thrust force and power. A detailed explanation of the stochastically forced linearised Navier-Stokes equations around a 2D base flow is provided.
- Chapter 4 elaborates on the data available from high-fidelity simulations and our methods for the of information in shaping the stochastic forcing that excites a statistically consistent response from the linearized NS model and improves predictions of thrust force and power over wind farms.

- In chapter 5, we apply our model over a  $2D$  plane at hub-height on a  $4 \times 1$  cascade of wind turbine. The results highlight the capabilities of the model predicting quantities of interest, i.e., thrust force, power, and turbulence intensities, in comparison with the predictions of LES.

## CHAPTER 2

### ENGINEERING WAKE MODELS

Various approaches such as analytical models, computational fluid dynamics (CFD), wind-tunnel and field experiments have been used in order to provide insightful information about the flow in a wind farm. Large-eddy simulations that can accurately predict the turbulent boundary layer flow have aided the development of tools for validation of wind farm technologies. Although the results of high-fidelity models are useful in analyzing the physics of turbulent wakes, they are only possible with help of large computational power and their accurate simulation require time on the order of days. Analytical wake models provide the basis for reduced order models that provide more flexibility and agility in analyzing flow field data.

Several models derived on simple laws of conservation, referred as engineering wake models, have been proposed in the literature. The key feature of these models is their low complexity which makes them an ideal candidate for layout optimization and control of wind farms. To start with the understanding of analytical models, we first describe the actuator disk model (ADM) for representing the wind turbine [14, Chapter 3]. The ADM represents the rotor as a porous disk that extracts kinetic energy from the wind reducing its velocity. Upon analysing the flow around the disk along a stream-tube (see Fig. 2.1), we can see that energy extraction process results in the expansion of the streamtube in the wake of the turbine. The energy extraction process within a control volume around the actuator disk yields the following expressions for the exerted thrust force and extracted power:

$$F = \frac{1}{2} \rho A C_T \mathbf{u}^2, \quad P = \frac{1}{2} \rho A C_P \mathbf{u}^3.$$

Here,  $F$  is the thrust force,  $P$  is the power,  $\rho$  is the air density,  $A$  is the area of the rotor disk,  $\mathbf{u}$  is the effective surface-averaged velocity on the rotor disk, and  $C_T$  and  $C_P$  are, respectively, thrust and power coefficients that can be defined as functions of the axial induction factor:

$$C_T = 4a(1 - a), \quad C_P = 4a(1 - a)^2.$$

The maximum value of  $C_P$ , which characterizes the Betz limit for turbine efficiency, is obtained with  $a = 1/3$  as 0.593 [14]. The energy generation in a wind farm can be estimated using these equations. However, in order to accurately predict these quantities, we need to compute the wind velocity within the farm. As explained earlier, the energy extraction by the wind turbine results in the development of a region of extremely low wind speeds

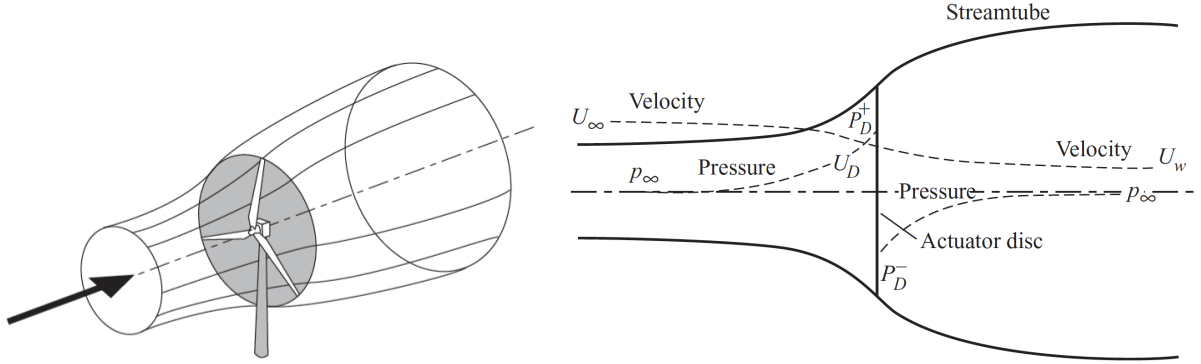


Figure 2.1: The actuator disk model (ADM). The rotor is considered as a porous disk that extracts the kinetic energy from the wind while reducing the wind velocity [14].

downstream of the turbine known as the wake. This region can be further classified into near wake and far wake regions. Near wake region is the highly turbulent region behind the turbine lasting roughly up to 5 diameter distance downstream. The flow in this region is dominated by the geometry of the turbine i.e. the tip-speed ratio (TSR) and the blade pitch angle. The far wake region is comparatively less turbulent as the pressure gradient becomes less significant and recovery in the speed due to the inter-mixing of the surrounding wind is observed. The far wake usually begins after 5 diameter downstream of a turbine. Based on this understanding of the wakes, various analytical approaches that model the shape of the wake thus, providing a relationship for the wind velocity. We now discuss some of the wake models.

## 2.1 Wake modeling based on co-flowing jets

One of the first interpretations of a wind turbine wake was proposed by Lissaman [63]. The idea was based on the theory of coflowing jets [1] wherein two distinct regions of the wake can be defined, the initial region of constant velocity potential core exist and the other far downstream. The potential core in the initial region is considered to have uniform velocity and radius  $r_c$ , while the velocity outside the core is defined by a characteristic shear layer. The core velocity  $U$  in the near wake region is given by the relation

$$\frac{U}{U_\infty} = \begin{cases} \frac{1}{m}; & 0 < r < r_c \\ \frac{1}{m} + \frac{m-1}{m(1-\eta^{1.5})^2}; & r_c < r < R \end{cases}$$

where,  $m$  is the ratio of outer flow velocity and spatially free-stream velocity ( $U_\infty$ ),  $r$  is the distance for the core centerline,  $R$  is the effective outer radius of the wake,  $(R - r_c)$  is the width of the turbulent mixed zone, and  $\eta = (r - r_c)/(R - r_c)$ . In the far wake region the velocity is obtained based on a static deficit as a factor of  $\xi = r/R$

$$\frac{U}{U_\infty} = 1 - U_\infty(1 - \xi^{1.5})^2$$

Based on these relationships, it is possible to obtain the velocity profile within a farm. It is important to note that a strong assumption of self similarity in both the wake regions is made.

## 2.2 Park Model

The Park model [57], developed as an extension of the Jensen model [48], incorporates wake superposition for velocity in the farm. It is one of the earliest proposed wake model. The simple nature of this model has made it a popular choice in many wind farm control strategies in the literature. The model assumes a uniform deficit (i.e. top-hat) for the velocity within all location in a uniformly expanding wake (see Figure 2.2). The reason for this representation of deficit was to depict the energy content accurately rather than describing the velocity field. The velocity behind a turbine at a downstream distance  $x$  is calculated using the relation

$$U = U_\infty \left[ 1 - \frac{2}{3} \left( \frac{r_0}{r_0 + \alpha x} \right)^2 \right]$$

where,  $r_0$  is the rotor diameter,  $\alpha$  is a tuneable nondimensional constant for wake parameterization. The relation is obtained by applying the conservation of momentum and neglecting the near wake turbulence. The velocity just behind the turbine is assumed to be  $\frac{1}{3}U_\infty$ . This is a very crude assumption as the velocity behind the turbine is dependent on the turbine calibrations, however, there is a reasonable correlation in the far wake regions with SCADA data or the high-fidelity simulations. Although the model provides a good representation of the wake, the top-hat deficit is a slight oversimplification of the reality.

## 2.3 Eddy viscosity model

A more detailed approach to understanding the wake is described in [3]. The wake is considered to be axisymmetric, turbulent and with zero circumferential velocities. In the far wake

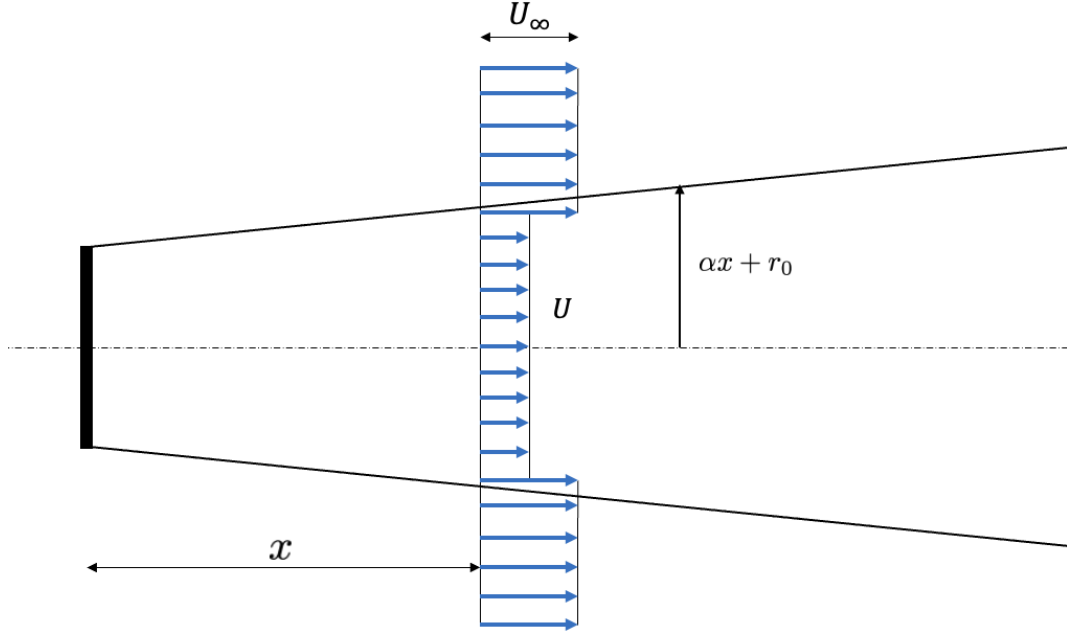


Figure 2.2: Schematic representing the top-hat approach for modeling the wake. The turbine is represented with thick black line and the uniformly growing wake profile is shown about the center line (dashed)

region, where the pressure gradient is negligible, the NS equation can be replaced with its equivalent thin layer approximation and the viscous term dropped yielding

$$U \frac{\partial U}{\partial x} + V \frac{\partial U}{\partial r} = -\frac{1}{r} \frac{\partial(r \overline{uv})}{\partial r}$$

where  $U$  and  $V$  are the streamwise and spanwise velocity respectively, and  $\overline{uv}$  are the shear stresses. The eddy viscosity is defined by

$$-\overline{uv} = \epsilon \frac{\partial U}{\partial r}; \quad \epsilon = l_w(x) U_w(x) + \epsilon_a$$

where  $l_w$  and  $U_w$  are the suitable length and velocity scales describing the wake shear layer and  $\epsilon_a$  is the ambient turbulence contribution to the eddy viscosity. Using the eddy viscosity model for wake deficit, a new model named as dynamic wake meandering (DWM) model has been proposed [60]. The model provides a unifying solution for analysing the power production and loading conditions on the turbine. The wake deficit and turbulence models are solved a priori and combined with the aeroelastic model FAST to analyse the turbine response. The DWM model is slower as compared other analytical model and is not suitable for implementation of feedback control as it calculates the flow field for each turbine for the entire simulation time.

## 2.4 Gaussian deficit model

Through the studies of bluff bodies in free stream flows, it was observed that the wake exhibited a self-similar Gaussian profile of the velocity deficit in the far-wake regions. Based on this information, authors in [8] proposed Gaussian deficit model for the wake behind a wind turbine. The velocity is given as

$$U = U_\infty \left[ 1 - C(x)e^{-\frac{r^2}{2\sigma^2}} \right]$$

where  $C(x)$  represents the maximum normalized velocity deficit at each downwind location along the center of the wake,  $r$  is the radial distance from the center of the wake, and  $\sigma$  is the standard deviation of the Gaussian-like velocity profile at each  $x$  location.

Assuming a linear expansion of the wake,  $\sigma$  can be expressed as

$$\frac{\sigma}{d_0} = k^* \frac{x}{d_0} + \epsilon$$

here  $k^*$  is the constant parameter representing the wake growth rate ( $\partial\sigma/\partial x$ ). The normalized velocity deficit is thus calculated using the relation

$$\frac{\Delta U}{U_\infty} = \left( 1 - \sqrt{1 - \frac{C_T}{8 \left( k^* \frac{x}{d_0} + 0.2\sqrt{\beta} \right)^2}} \right) e^{\left( -\frac{1}{2 \left( k^* \frac{x}{d_0} + 0.2\sqrt{\beta} \right)^2} \left( \frac{y}{d_0} \right)^2 + \left( \frac{z}{d_0} \right)^2 \right)} \quad (2.1)$$

where  $\Delta U = U_\infty - U$  is the velocity deficit, and  $x, y, z$  are the distances in the streamwise, wall normal and spanwise directions from the wake center line. In order to obtain an accurate velocity field it is important to tune the parameters precisely. It has been shown with the help of field data, relationships based on the incoming turbulence intensity (TI) can be obtained to decide the constants [117].

## 2.5 Wake superposition

Another phenomenon that is witnessed in a wind farm is the overlap between wakes of two individual turbines. Analytical wake models account for this through superposition of deficits. The approach involves calculating the velocity at each location in the farm and then apply superposition to account for the interactions between overlapping wakes. Although the



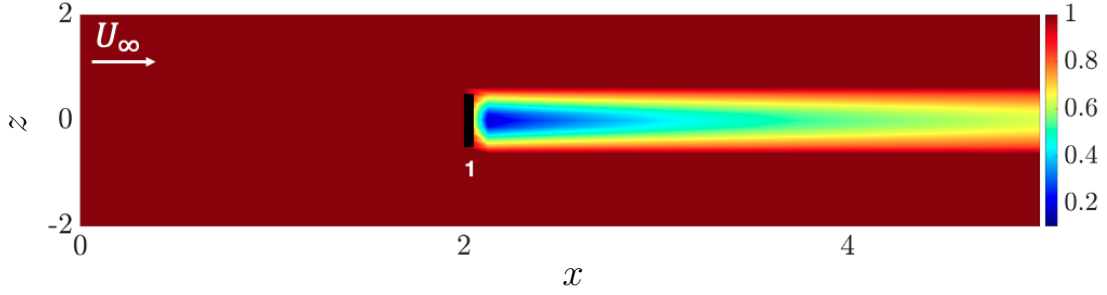


Figure 2.3: The normalized wake velocity using the Gaussian profile for the deficit calculated using Eq. 2.1. The turbine is indicated with the thick black line.

overlapping of wakes may increase the turbulence and affect the performance of the downwind turbines, this phenomenon can be utilized to identify the cluster of turbines that need to be coordinated to maximize the power extraction. Since the very first study involving analysis of wake through jet theory Sec. 2.1, different superposition methods have been proposed. The difference in the methods originates from their use of either linear superposition of velocity deficit (Eq. 2.2) or linear superposition of energy deficit (Eq. 2.3).

$$U(x, y, z) = U_\infty - \sum_{i=1}^n \Delta U_i(x, y, z) \quad (2.2)$$

$$U(x, y, z) = U_\infty - \sqrt{\sum_{i=1}^n \Delta U_i^2(x, y, z)} \quad (2.3)$$

where the subscript ( $i = 1$  to  $n$ ) denotes the velocity deficit induced by all the upwind turbines with wake overlap at the given location  $X(x, y, z)$ .

## 2.6 Shortcomings of the analytical wake models

Although the analytical wake models are useful for wind-farm layout optimization, they neglect the time-varying near-field turbulence behind the wind turbine and when combined with linear wake superposition laws they provide an over-simplified prediction of wake velocities under steady atmospheric conditions. In the absence of a turbulence model that can capture the effect of the ABL and rotor-induced mixing, velocity deficits predicted by such models are typically over-predicted, and thus, lead to inaccurate predictions of the load and power (Figure 3.1).

Following a similar approach as the ADM with rotation from Porté-Agel et al. [78] and Wu and Porté-Agel [110], the thrust force and power can be computed as the aggregate of

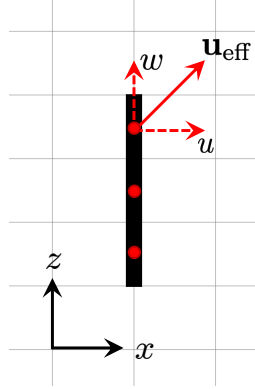


Figure 2.4: Geometric sketch of a 2D grid of collocation points around a turbine rotor. The sample grid demonstrates the division of the turbine rotor into 3 equally sized segments. The staggered points where the effective velocities  $\mathbf{u}_{\text{eff}}$  and the intensities used in Equations (3.2) are computed are marked by the red dots.

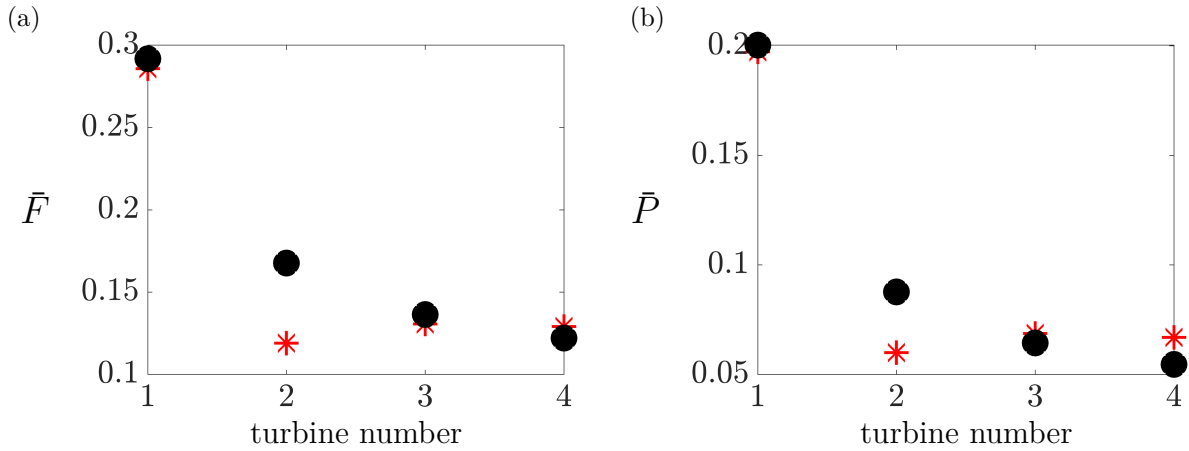


Figure 2.5: (a) Predictions of thrust force  $\bar{F}$  and (b) power generation  $\bar{P}$  from LES (\*) and the result of using Equation (2.4) with 15 segments across the spanwise extent of turbine rotors (see Fig. 2.4) and the velocity field predicted by the analytical model (5.2) (•).

contributions from constituting segments of a turbine rotor resulting from the discretization of the spatial domain, i.e.,  $F = \sum_i F_i$  and  $P = \sum_i P_i$ , where

$$F_i = \frac{1}{2} \rho A_i C_T \mathbf{u}_{\text{eff},i}^2, \quad P_i = \frac{1}{2} \rho A_i C_P \mathbf{u}_{\text{eff},i}^3. \quad (2.4)$$

Here,  $A_i$  represents the area of the rotor disk segment and  $\mathbf{u}_{\text{eff},i}$  represents the effective velocity over the  $i$ th segment, which may be computed as the resultant velocity field evaluated on a staggered grid; see Figure 2.4 for an illustration.

A solution to this could be to analyse medium fidelity models such as those that are based on the Reynolds-averaged NS equations (RANS) or eddy viscosity. These models are not prone to similar issues as they capture the 3D dynamic variation of the velocity field and introduce turbulence models that enable wake recovery [45, 10]. A downside however, is the computational demands. We take a step in compensating the shortcomings of low-fidelity models via reduced-order modeling of second-order statistics of the velocity field that are pertinent in the prediction of thrust force and power for various turbines using turbulence intensities in accordance with field measurements or LES results. To this end, we adopt the stochastic dynamical modeling framework of Zare et al. [111, 115, 112] to model the effect of background turbulence using linear dynamical models and improve the predictive capability of low-fidelity engineering models without adding to their dimensional complexity (Figure 6.1). The resulting data-enhanced models are of low-complexity and are thus convenient for conducting linear stochastic simulations. They are also well-suited for analysis and synthesis using tools from modern robust control as they provide an explicit linear state-space representation for the dynamics of velocity fluctuations in wind farms.

In this chapter, we discussed the various low-fidelity analytical models that can be utilised to obtain the velocity field in a wind farm. While these models are simple and provide accurate representation of the velocity in the far wake, they over predict the deficit and do not capture the trend of prediction for thrust force and power. In the next chapter we present our approach for introducing a degree of freedom to augment the predictions of quantities. We also introduce the linearized Navier-Stokes equations that govern the dynamics of flow fluctuations around a base flow profile informed by analytical wake models.

## CHAPTER 3

### STOCHASTICALLY FORCED LINEARIZED NAVIER-STOKES

The wind velocity field  $\mathbf{u}$  in the farm can be decomposed into the sum of a time-averaged mean  $\bar{\mathbf{u}}$  and zero-mean fluctuations  $\mathbf{v}$  as

$$\mathbf{u} = \bar{\mathbf{u}} + \mathbf{v}, \quad \bar{\mathbf{u}} = \mathbf{E}[\mathbf{u}], \quad \mathbf{E}[\mathbf{v}] = 0 \quad (3.1)$$

where overline and  $\mathbf{E}[\cdot]$  both denote the time-average operator, e.g.,

$$\bar{\mathbf{u}}(\mathbf{x}) = \mathbf{E}[\mathbf{u}(\mathbf{x}, t)] = \lim_{T \rightarrow \infty} \frac{1}{T} \int_0^T \mathbf{u}(\mathbf{x}, t + \tau) d\tau.$$

Here,  $\mathbf{x}$  denotes the spatial coordinates and  $t$  is time. The velocity fluctuation field  $\mathbf{v}$ , which we will use to capture the effect of atmospheric turbulence on the wake model, is assumed to be a stochastic Gaussian process. When the velocity incident on the turbines is perpendicular to the rotor and there is no cross-wind, substitution of Equation (3.1) into Equation (2.4) yields the following equations for the time-averaged thrust force and power associated with  $i$ th segment of the rotor:

$$\bar{F}_i = \frac{1}{2} \rho A_i C_T \left( \bar{\mathbf{u}}_{\text{eff},i}^2 + \overline{\mathbf{v}_{\text{eff},i}^2} \right) \quad (3.2a)$$

$$\bar{P}_i = \frac{1}{2} \rho A_i C_P \left( \bar{\mathbf{u}}_{\text{eff},i}^2 + \overline{\mathbf{v}_{\text{eff},i}^2} \right)^{3/2}, \quad (3.2b)$$

where the effective velocities can represent the resultant of their components, e.g.,  $\mathbf{v}_{\text{eff}} = \sqrt{u^2 + w^2}$  when  $\mathbf{v} = [u \ w]^T$ , and the stochastic properties of the fluctuation field  $\mathbf{v}$ , namely its zero mean (cf. Equation (3.1)) and skewness (due to its Gaussian distribution), have been used to eliminate certain terms. Based on Equations (3.2), the scalar quantities that we obtain for the thrust force and power of each turbine are functions of not only the effective mean velocity  $\bar{\mathbf{u}}$ , but also the second-order statistics of the fluctuation field  $\mathbf{v}$  at the staggered points of the discretization grid. While analytical models provide a static prediction of the effective velocity in the wind farm (similar to  $\bar{\mathbf{u}}$ ), the fluctuation field  $\mathbf{v}$  provides an additional dynamic degree-of-freedom whose second-order statistics can be modeled to improve predictions of flow quantities across the farm; given a set of available time-averaged thrust force  $\{\bar{F}_i\}$  and power  $\{\bar{P}_i\}$  measurements for various turbines, the dynamics of  $\mathbf{v}$  can be sought to augment the predictions of static analytical models by providing the necessary second-order statistics  $\overline{\mathbf{v}_{\text{eff}}^2}$  for matching the available data (cf. Equations (3.2)). On

the other hand, the statistics of  $\mathbf{v}$  may be directly modeled to match turbulence intensities across the wind farm.

A number of options exist for modeling velocity fluctuations  $\mathbf{v}$  including data-driven approaches. Herein, we follow the stochastic dynamical modeling approach of Zare et al. [111, 115, 112] and pursue stochastically forced linear time-invariant (LTI) approximations of complex wind farm flow dynamics. Specifically, we assume the following state-space representation

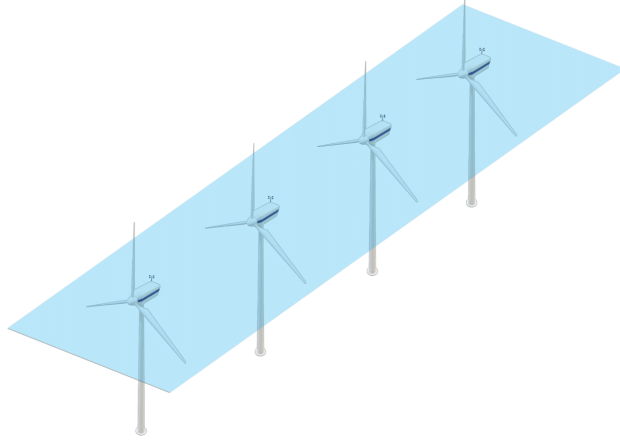
$$\begin{aligned}\psi_t(\mathbf{x}, t) &= \mathbf{A} \psi(\mathbf{x}, t) + \mathbf{B} \mathbf{d}(\mathbf{x}, t) \\ \mathbf{v}(\mathbf{x}, t) &= \mathbf{C} \psi(\mathbf{x}, t)\end{aligned}\tag{3.3}$$

for the dynamics of velocity fluctuations  $\mathbf{v}$ , where  $\psi$  is the state vector,  $\mathbf{d}$  is a stationary zero-mean stochastic process,  $\mathbf{A}$  is the dynamic generator that represents the prior dynamical representation for the turbulent flow dynamics,  $\mathbf{B}$  is the input operator that is used to introduce the input  $\mathbf{d}$  into the dynamics,  $\mathbf{C}$  is an output operator that relates the state  $\psi$  to the output velocity field  $\mathbf{v}$ , and  $(\cdot)_t$  is the partial derivative with respect to time. In this thesis, we focus on physics-based dynamical approximations resulting from linearization of the NS around static base flow profiles that are generated by conventional engineering models. Nonetheless, alternative linear models, which may result from application specific assumptions/simplifications, or data-driven methods such as dynamic mode decomposition [5, 56, 90, 89] may also provide viable starting points for our modeling framework. Together with the prior low-fidelity engineering model that predicts  $\bar{\mathbf{u}}$ , the dynamical model considered for velocity fluctuations  $\mathbf{v}$  gives rise to a class of low-complexity models that are more accurate in predicting quantities that depend on turbulent flow statistics, but maintain a lower dynamic complexity relative to medium-fidelity models (Figure 6.1).

### 3.1 Linearized Navier-Stokes

In this section, we establish the governing physics of the wind farm which can be modeled into the form of a linear system. The Navier-Stokes equations are the reference for any form of fluid flow but they demand computational power over a long duration to provide satisfactory results. In order to develop a reduced order model for the wind farm, we utilise our augmented velocity to linearize the NS equations around a static velocity profile  $\bar{\mathbf{u}}$  that is generated by a low-fidelity engineering wake model. Our focus will be on 2D models of wind farm turbulence that are constrained to planes at the hub height of wind turbines. We

(a)



(b)

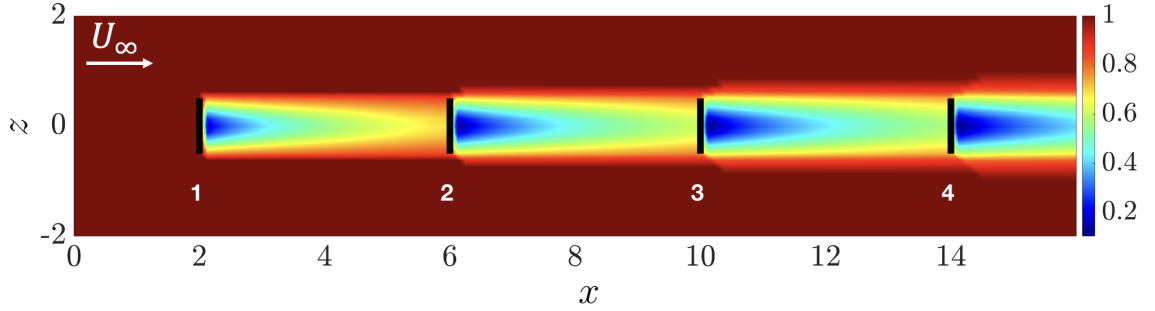


Figure 3.1: (a) A cascade of 4 equally spaced turbines. (b) The streamwise and spanwise dependence of the velocity field  $\bar{\mathbf{u}}(x, z)$  generated by the analytical model (5.2) from Bastankhah and Porté-Agel [8] over the 2D computational domain at hub height. The thick black lines mark the location of the turbine rotors.

note, however, that the proposed modeling framework is readily generalizable to 3D wind farm models that account for the remaining wall-normal dimension.

The dynamics of small velocity and pressure fluctuations  $(\mathbf{v}, p)$  around the base flow profile  $(\bar{\mathbf{u}}, \bar{P})$  are governed by the linearized NS and continuity equations

$$\begin{aligned} \mathbf{v}_t &= -(\nabla \cdot \mathbf{v}) \bar{\mathbf{u}} - (\nabla \cdot \bar{\mathbf{u}}) \mathbf{v} - \nabla p + \frac{1}{Re} \Delta \mathbf{v} - K^{-1} \mathbf{v} + \mathbf{d} \\ 0 &= \nabla \cdot \mathbf{v} \end{aligned} \quad (3.4)$$

where the vector  $\mathbf{v} = [u \ w]^T$ , with  $u$  and  $w$  denoting components of fluctuating velocity field in the streamwise ( $x$ ) and spanwise ( $z$ ) directions, respectively,  $\nabla$  is the gradient operator,  $\Delta = \nabla \cdot \nabla$  is the Laplacian operator, and the Reynolds number  $Re = U_\infty d_0 / \nu$  is defined

in terms of the rotor diameter  $d_0$ , the free-stream velocity  $U_\infty$ , and the kinematic viscosity  $\nu$ . All variables in Equation (3.4) have been non-dimensionalized: length by  $d_0$ , velocity by  $U_\infty$ , time by  $d_0/U_\infty$ , and pressure by  $\rho U_\infty^2$ . In Equation (3.4),  $\mathbf{d}$  represents an additive zero-mean stationary stochastic input that triggers a statistical response of the linearized dynamics.

A standard conversion for the elimination of pressure together with finite-dimensional approximation of the differential operators brings the linearized equations (3.4) into the form of the evolution model

$$\dot{\mathbf{v}}(t) = A \mathbf{v}(t) + B \mathbf{d}(t) \quad (3.5)$$

### 3.2 Volume penalization technique

In Equation (3.4), the volume penalization term  $K^{-1}\mathbf{v}$  is used to capture the effect of turbine rotors and nacelles (and even turbine towers in 3D models) on the velocity field. This method avoids the implementation of boundary conditions in complex geometries by modeling the effect of solid obstructions of the flow as a spatially varying permeability function  $K$  that influences the governing equations as an additive body force. Within the fluid, the penalization resulting from the permeability function  $K$  should have no influence on the flow, i.e.,  $K \rightarrow \infty$ , yielding back the original linearized NS dynamics for  $\mathbf{v}$ . On the other hand, within solid structures, the function  $K$  should force the velocity field to zero, i.e.,  $K \rightarrow 0$ ; see [58] for details. We note that this method was recently used to account for the presence of spanwise periodic surface corrugation (riblets) in turbulent channel flow [80]. To capture the spatial region that is influenced by the presence of the turbines, we use a smooth 2D filter function of the form:

$$K^{-1}(x, z) = \frac{c}{\pi^2} [\text{atan}(a(x - x_1)) - \text{atan}(a(x - x_2))] \times [\text{atan}(a(z - z_1)) - \text{atan}(a(z - z_2))], \quad (3.6)$$

where  $x_{1,2}$  and  $z_{1,2}$  determine the spatial extent of the rotors in the horizontal directions and parameters  $a$  and  $c$  determine the slope and magnitude of the function, respectively; see Figure 3.2 for samples of 1D and 2D resistance functions  $K^{-1}$ . Typically, the slope  $a$  is set to a reasonably large value that clearly captures the spatial extent of the turbines but does not violate differentiability or cause large derivatives of  $K^{-1}$  in the linearized operator. Depending on the arrangement of the farm and the orientation of the turbine to the incoming

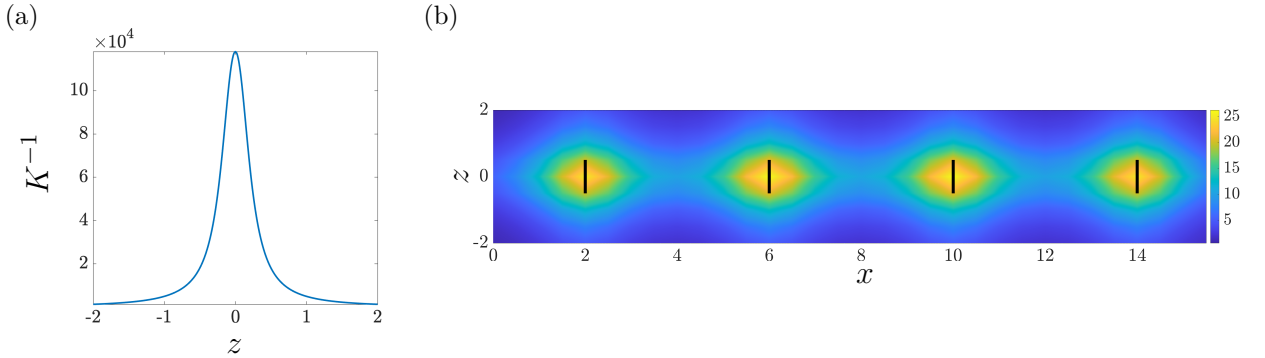


Figure 3.2: (a) The spanwise dependence of the resistance function  $K^{-1}(z)$  following Equation (3.6) with  $z_1 = -0.1$ ,  $z_2 = 0.1$ ,  $a = 5$ , and  $c = 400$ . (b) The streamwise and spanwise dependence of the resistance function  $K^{-1}(x, z)$  corresponding to Equation (3.6).

wind, the parameters in the resistance function need to be tuned. Ideally, the magnitude  $c$  would be set to extremely large values to ensure a significant drop in the velocity field within the turbine structures. However, in practice, large values of  $c$  can violate stability of the linearized NS operator. In Fig. 3.3 we show the effects of increasing intensity on the eigen spectrum of the dynamic matrix  $A$ . Starting with absence of turbines with the domain (i.e.  $c = 0$ ), Fig. 3.3(a) indicates that the flow is marginally stable (eigenvalues of  $A$  in Equation (3.3) fall on the imaginary axis). As we keep increasing the parameter, we observe the dominant branches that represent the dominant frequencies in the flow (Fig. 3.3(b - e)). A threshold is observed beyond which increasing the intensity results in instability indicating the boundary value for the tuning parameter (Fig. 3.3(f)). Setting the parameter value at the threshold enables the system to identify the key features (i.e. statistical signatures) in the wake of the turbine. The system response in terms of identifying the features can also be studied based on response to white noise forcing, however, the peaks of the features are amplified and hence, we need to identify a colored-in-time forcing. For the case of our numerical experiments in Chapter. 5, a value of  $c = 184$  was found to be the threshold.

### 3.3 Second-order statistics of LTI systems

For system (3.5) with Hurwitz  $A$  and controllable pair  $(A, B)$ , a matrix  $X$  qualifies as the steady-state covariance matrix of the state vector, i.e.,

$$X := \lim_{t \rightarrow \infty} \mathbf{E}(\boldsymbol{\psi}(t) \boldsymbol{\psi}^*(t)),$$



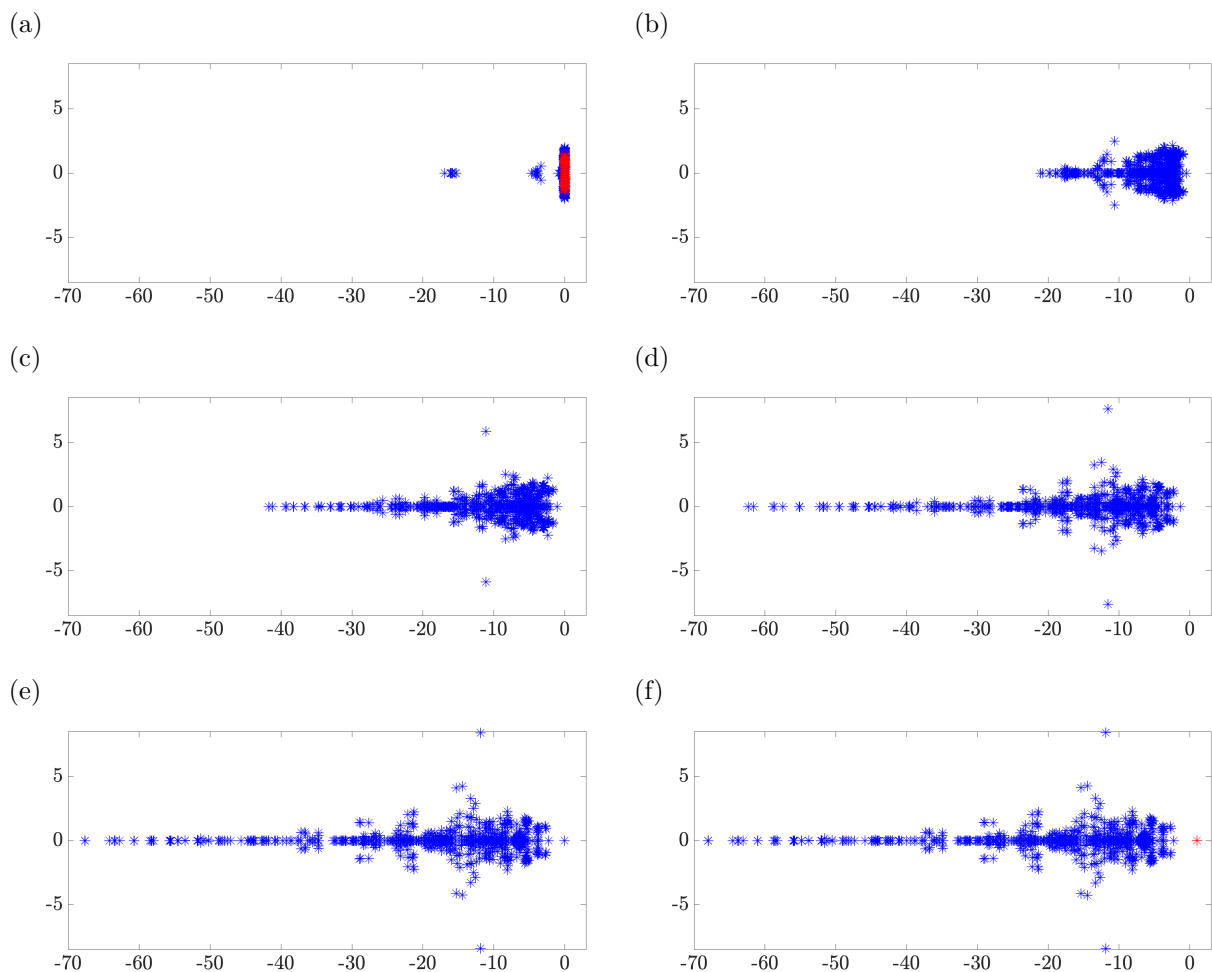


Figure 3.3: The eigen spectrum analysis of the dynamic generator  $A$  with tuneable parameter (a)  $c = 0$ , (b)  $c = 50$ , (c)  $c = 100$ , (d)  $c = 150$ , (e)  $c = 184$ , (f)  $c = 185$  in the resistance function Eq. 3.6. (\*) are stable eigen values and (\*) denoting the unstable eigen values.

if and only if the Lyapunov-like equation

$$AX + XA^* = -BH^* - HB^* \quad (3.7)$$

is solvable for the matrix  $H$  [35, 34]. Here,  $*$  denotes the complex conjugate transpose. The matrix  $H$  quantifies the cross-correlation between the input and the state in model (3.5) [115, Appendix B]:

$$H := \lim_{t \rightarrow \infty} \mathbf{E}[\psi(t)\mathbf{d}^*(t)] + \frac{1}{2}B\Omega.$$

When the stochastic input  $\mathbf{d}$  is zero-mean and white-in-time (state-independent) with covariance  $\Omega$ ,  $H = (1/2)B\Omega$  reduces Equation (3.7) to the standard algebraic Lyapunov equation (3.8). In contrast to the Lyapunov Equation (3.8), the right-hand side of Equation (3.7)

is in general sign indefinite, i.e., will have both positive and negative eigenvalues unless the stochastic forcing  $\mathbf{d}$  is white-in-time. The one-point velocity correlations along the diagonal of the state covariance matrix  $X$  constitute turbulence intensities that are either matched in accordance with field measurements across the farm or model the deficits in matching thrust force or power generation in accordance with the segmented ADM model (3.2).

For the wind farm flow under steady atmospheric conditions, the global operator in Equation (3.5) has no exponentially growing eigenmodes (i.e., the dynamic matrix  $A$  is stable). Thus, the steady-state covariance of the fluctuating velocity field

$$X := \lim_{t \rightarrow \infty} \mathbf{E}(\mathbf{v}(t) \mathbf{v}^*(t)),$$

subject to zero-mean white-in-time forcing  $\mathbf{d}$  with spatial covariance matrix  $\Omega \succeq 0$ , i.e.,  $\mathbf{E}(\mathbf{d}(t)) = 0$  and  $\mathbf{E}(\mathbf{d}(t) \mathbf{d}^*(\tau)) = \Omega \delta(t - \tau)$  can be obtained from the solution to the Lyapunov equation,

$$AX + XA^* = -B\Omega B^*. \quad (3.8)$$

The Lyapunov equation (3.8) relates the statistics of white-in-time forcing, represented by  $\Omega$ , to the infinite-horizon state covariance  $X$  via system matrices  $A$  and  $B$ . The energy spectrum of the streamwise and spanwise velocity components can be extracted from the diagonal entries of the matrix  $X$  and the total kinetic energy of the flow can be computed as  $E = \text{trace}(X)$ . While white-in-time forcing is useful in studying the receptivity of the turbulent flow to exogenous disturbances [55, 79], it is often found to be insufficient in reproducing its statistical signatures [115, 112]. To address this issue, we next consider the more general case of colored-in-time stochastic forcing, and pose inverse problems that identify both the statistics of colored-in-time forcing and an input matrix  $B$  to match available second-order statistics of wind farm turbulence using the LTI model (3.5).

In this chapter, we introduced our approach for enhancing the predictions in a wind farm with the help stochastically forced linear dynamics which are the linearized NS equations linearized around a base flow velocity informed by the analytical wake models. The state-space representation of these dynamics solve for the small fluctuations around the mean velocity in a farm. Next we discuss the statistics quantities in a wind farm flow and how we can obtain the stochastic forcing to excite the linear dynamics to reproduce these statistics.

## CHAPTER 4

### STOCHASTICAL DYNAMICAL MODELING OF PARTIALLY AVAILABLE STATISTICS

Modern-day wind farms use a host of sensing devices that are distributed across the farm to provide critical SCADA data for assessing the performance of the power plant and make changes to the operational settings of wind turbines in real time. The incoming stream of flow measurements from nacelle mounted anemometers, weather towers, pressure sensors, or even Doppler LiDAR systems can be processed to determine the power extracted by turbines, loads exerted on rotor structures, and the direction and speed of the incoming wind. Time averaged quantities can also be used to develop wake models that may in turn enable model-based flow estimation and wind farm control synthesis. Restricted by the modeling premise afforded by the segmented ADM model, herein, we utilize such data to realize stochastic forcing models for the linearized NS equations (3.5) that yield output velocity statistics that best reproduce the quantities of interest. We consider the availability of two types of data: (i) power and thrust force measurements at turbines; and (ii) velocity intensities at prespecified locations across the wind farm. While the second type of data (second-order statistics of the fluctuating velocity field  $\overline{\mathbf{v}^2}$ ) directly specifies entries in the covariance matrix  $X$  of the linearized model (3.5), the first type only provides such statistics through the ADM model; given time-averaged thrust force or power generation measurements across the farm, we use Equations (3.2) together with a static approximation of an analytical wake model to obtain the resultant turbulence intensity at staggered points across the rotor structure and predict the competing quantity. Note that due to a lack of sufficient degrees of freedom in Equations (3.2), both thrust force and power measurements cannot be simultaneously matched. Details of how we obtain the turbulence intensity to match power or thrust force measurements or a balanced approximation of the two that addresses the issue of insufficient degrees of freedom are provided in Sec. 5.4. Either of the three scenarios covered in the section yield an effective velocity intensity for each staggered point across the turbine rotors, but do not provide information regarding the contributions from different velocity components (e.g.,  $u^2$  or  $w^2$ ), which may be provided via additional problem specific information such as the rotor yaw angle. Moreover, assuming knowledge of power and thrust force over individual segments of turbine rotors may not be a realistic expectation unless sensors are mounted on the surface of turbine blades. Consideration of scenarios where power or thrust force measurements are provided for entire turbines or turbine rotors are

misaligned with the incoming wind direction is a topic of ongoing research. In Section 5.4, we demonstrate how access to thrust force (power) measurements can result in predictions of power generation (thrust force) for wind turbines, and in Section 5.5, we demonstrate how partially observed second-order statistics of the velocity field can be used to complete the second-order statistical signature of the wind farm turbulence.

Partially available second-order statistics of the velocity field  $\overline{\mathbf{v}^2}$  denote a subset of entries of the state covariance matrix  $X$ , which we wish to model. In the remainder of this section, we provide background material regarding the structural constraints on the state covariance matrix  $X$ , draw from the stochastic dynamical modeling framework of Zare et al. [111, 115, 112] to formulate covariance completion problems that identify the statistics of stochastic forcing  $\mathbf{d}$  into linear Gaussian model (3.5) to reproduce the available second-order statistics  $\mathbf{v}^2$ , and provide details of a filter parameterization that enable the stochastic realization of the identified forcing.

#### 4.1 Covariance completion

Given partially known diagonal entries of  $X$  corresponding to deficits in matching thrust force, power generation, or turbulence intensities across the farm, we seek an input matrix  $B$  and statistics of forcing  $\mathbf{d}$  that are consistent with the hypothesis that the required statistics in  $\mathbf{v}$  are generated by model (3.5) with known generator  $A$ . It is also important to restrict the complexity of the identified forcing model, which is quantified as the number of degrees of freedom that are directly influenced by the stochastic forcing, i.e., the number of input channels in matrix  $B$  or  $\text{rank}(B)$ . To these ends, we follow Zare et al. [111, 115, 112] in solving the structured covariance completion problem:

$$\begin{aligned}
& \underset{X, Z}{\text{minimize}} && -\log \det(X) + \gamma \|Z\|_* \\
& \text{subject} && AX + XA^* + Z = 0 \\
& && X \circ E - G = 0
\end{aligned} \tag{4.1}$$

which penalizes a composite objective subject to two linear constraints with the first corresponding to the Lyapunov-like equation (3.7) and the second denoting the set of known second-order statistics of the velocity field. Here, the matrices  $A$ ,  $C$ ,  $E$ , and  $G$  are problem data, and the Hermitian matrices  $X$ ,  $Z$  are optimization variables. Entries of  $G$  represent partially available second-order statistics of the velocity field  $\mathbf{v}$ , the symbol  $\circ$  denotes

elementwise matrix multiplication, and  $E$  is the structural identity matrix,

$$E_{ij} = \begin{cases} 1, & \text{if } G_{ij} \text{ is available} \\ 0, & \text{if } G_{ij} \text{ is unavailable.} \end{cases}$$

The objective function provides a trade-off between the solution to a maximum-entropy problem and the complexity of the forcing model; the logarithmic barrier ensures the positive definiteness of the matrix  $X$  and the nuclear norm regularizer, which is weighted by the parameter  $\gamma > 0$ , is used as a proxy for the rank function (see, e.g., References [29, 82]). The rank of the matrix  $Z$  bounds the number of independent input channels or columns in matrix  $B$ ; for details see [111]. We note that unless the forcing  $\mathbf{d}$  in Equation (3.5) is white-in-time, the matrix  $Z$  may have both positive and negative eigenvalues. Convex optimization (4.1) can be cast as a semidefinite program and solved efficiently using standard solvers [102, 38, 13] for small- and medium-size problems. In [113, 111], customized algorithms have been developed to deal with larger problems such as those arising in the modeling of multi-turbine wind farms.

## 4.2 Stochastic realization

Problem (4.1) combines the nuclear norm with an entropy function in order to target low-complexity structures for stochastic forcing and facilitate the construction of a particular class of low-pass filters that generate suitable forcing into Equation (3.5). The solution  $Z$  to optimization problem (4.1) can be decomposed into matrices  $B$  and  $H$  (cf. Equation (3.7)) via spectral factorization. These factors, together with matrix  $X$  that also results from solving problem (4.1) and the state matrix  $A$  enable the construction of generically minimal linear filters that have the same number of degrees of freedom as system (3.5) and are given by:

$$\dot{\xi}(t) = (A - BK)\xi(t) + B\mathbf{w}(t) \tag{4.2a}$$

$$\mathbf{d}(t) = -K\xi(t) + \mathbf{w}(t) \tag{4.2b}$$

where,

$$K = \frac{1}{2}\Omega B^*X^{-1} - H^*X^{-1}. \tag{4.2c}$$

Here,  $\xi$  is the state of the filter and  $\mathbf{w}$  is a zero-mean white-in-time stochastic process with covariance  $\Omega \succ 0$ ; see Figure 1.3. The minimal realization of the linear filter and linearized

dynamics results in a parsimonious (low rank) modification to the original linearized dynamics (Figure 1.3),

$$\dot{\boldsymbol{\psi}}(t) = (A - BK)\boldsymbol{\psi}(t) + B\mathbf{w}(t). \quad (4.3)$$

The resulting stochastic wake model is linear and maintains a close relation with the physics retained by the linearized NS equations due to the low-rank nature of the modification term  $BK$ . Thus, it is not only convenient for the purpose of conducting linear stochastic simulations and real-time model-based feedback control with provable performance guarantees, but it holds the promise to ensure satisfactory performance even when the real physical system deviates from the model used for design.

In this chapter we showed that covariance completion problem can be formulated as a covariance control problem that can identify the input matrix and the stochastic forcing for the LTI system to reproduce the second order statistics of the velocity field. Next we apply our modeling framework to a multi-turbine wind farm.

## CHAPTER 5

### STOCHASTIC DYNAMICAL MODEL FOR WIND FARMS

In this chapter, we utilize the stochastic dynamical modeling framework presented in Chapter 3 to account for partially available second-order statistics of the turbulent velocity field  $\mathbf{v}^2$  at the hub height of a wind farm. We begin with a brief discussion into the details of LES which were used to generate data for the training and verification/validation of our stochastic dynamical models. We demonstrate the capability of our models in improving the predictions of analytical wake models in capturing the thrust force and power generation over the turbines in the  $4 \times 1$  cascade shown in Figure 3.1. We then focus on a single turbine configuration to assess the value of velocity statistics at various distances downstream of the turbine in training our data-enhanced stochastic wake model. We build on the results obtained from this case study to model the turbulent flow impinging on a cascade of 4 turbines. Finally, we provide a dynamical realization for the identified stochastic forcing and conduct linear stochastic simulations to verify the ability of our models in accounting for statistical signatures of wind farm turbulence.

#### 5.1 Large-eddy simulations

A cascade of 4 NREL-5MW reference turbines [52] (Figure 3.1(a)) is simulated using the LES code UTD-WF [18, 20, 85, 87], which employs the rotating ADM to account for the effect of rotating turbine blades and the immersed boundary method of Orlandi and Leonardi [75] to account for the towers and nacelles. The computational box extends  $32 d_0$ ,  $10.24 d_0$  and  $10 d_0$  in the streamwise, spanwise, and vertical directions, respectively. The distance between the inlet and the most upstream turbine is equal to  $9 d_0$ . No-slip conditions are applied at the bottom boundary of the computational domain in addition to the surfaces of nacelles and towers, free-slip conditions are applied at the top boundary, periodic boundary conditions are imposed at the two spanwise sides, and radiative boundary conditions [76] are implemented at the outlet. The grid is stretched in the vertical direction in order to have a finer resolution in the regions where the turbine rotors are present; grid resolution in the refined sections with the turbines is uniform in all three directions,  $\Delta x = \Delta z = \Delta y = 0.025 d_0$ . Although the resolution is not sufficient to resolve the boundary layer flow around the tower accurately (as in most LES), the impermeability provided by the immersed boundary method reproduces blockage effects and overall momentum loss across the turbine structures.

In order to mimic the atmospheric boundary layer at the inlet, turbulence obtained from a precursor simulation is superimposed to a mean velocity profile expressed by the following

law:

$$\frac{U}{U_{\text{hub}}} = \left( \frac{y}{y_{\text{hub}}} \right)^\alpha, \quad (5.1)$$

where  $U$  is the streamwise velocity component at height  $y$ ,  $U_{\text{hub}} = U_\infty$  is the mean streamwise component of the wind velocity at hub height  $y_{\text{hub}}$ , and  $\alpha$  is the shear exponent, which we set to  $\alpha = 0.05$ . The upstream velocity  $U_\infty$  is chosen to be about  $0.8 U_{\text{rated}}$ . This allows using a standard region II control law[50, 59] for the rotor dynamics where each turbine is assumed to extract the maximal energy from the incoming flow. The precursor simulation is run in a computational box with periodic boundary conditions in both streamwise and spanwise direction, no-slip conditions at the bottom, and free-slip conditions at the top. Roughness cubes are placed on the ground (bottom of the computational domain) to enhance the generation of turbulence [61]. The superposition of the mean flow in Equation (5.1) and the turbulence from the precursor simulation results in a hub-height turbulence intensity of 8% impinging the first turbine in the cascade. The time-averaged and root mean square profiles of velocity fluctuations are computed using 750 instantaneous snapshots of the 3D velocity field generated by LES. The numerical experiments herein will consider a Reynolds number based on  $d_0$  and  $U_\infty$  equal to  $Re = 8 \times 10^7$  in accordance with the LES.

## 5.2 Base flow

Our stochastic models are based on the stochastically forced linearized NS equations around a static base flow profile  $\bar{\mathbf{u}}$  with an analytical expression provided by a low-fidelity engineering wake model. For simplicity, we assume all turbines to be facing the wind, i.e.,  $0^\circ$  yaw angle relative to the free-stream velocity, restrict the computational domain to the 2D space at hub height (Figure 3.1(a)), and assume zero cross-wind, which means that the base flow will only contain one non-zero component in the streamwise direction. For the base flow, we use the Gaussian deficit wake model discussed in Chapter. 2, where the velocity is given using the relation

$$\bar{\mathbf{u}}(x, z) = U_\infty - U_\infty \left( 1 - \sqrt{1 - \frac{C_T}{8 \left( k^* \frac{x}{d_0} + 0.2\sqrt{\beta} \right)^2}} \right) e^{\left( -\frac{1}{2 \left( k^* \frac{x}{d_0} + 0.2\sqrt{\beta} \right)^2} \left( \frac{z}{d_0} \right)^2 \right)} \quad (5.2)$$



where  $d_0 = 1$  is the non-dimensional diameter of turbines and  $k^* = 0.03$  is the wake growth rate, which we have chosen in accordance with earlier studies (e.g., [8], [117]). The choice of  $C_P = 0.485$  and  $C_T = 0.787$  correspond to the maximum power generated by a 5MW NREL turbine [51] using an LES code that leverages blade momentum element theory [86, 88]. When considering multi-turbine farms, we follow a linear superposition law to capture velocity deficits in the overlapping regions where wakes interact. Figure 3.1(b) shows the static 2D velocity field corresponding to Equation (5.2) for a cascade of 4 turbines, where we have used  $\Delta_x = \Delta_z = 0.125$  to discretize the horizontal dimensions.

### 5.3 System matrices in linearized NS equations in evolution form and boundary conditions

The system matrices in Equation (3.5) are given as

$$\begin{aligned}
A &= \Delta^{-1} \begin{bmatrix} A_{11} & A_{12} \\ A_{21} & A_{22} \end{bmatrix}, \\
B &= \Delta^{-1} \begin{bmatrix} \mathbf{f}_{zz} + 2\mathbf{f}_z \partial_z + \mathbf{f} \partial_{zz} & -(\mathbf{f}_{xz} + \mathbf{f}_x \partial_z + \mathbf{f}_z \partial_x + \mathbf{f} \partial_{xz}) \\ -(\mathbf{f}_{xz} + \mathbf{f}_x \partial_z + \mathbf{f}_z \partial_x + \mathbf{f} \partial_{xz}) & \mathbf{f}_{xx} + 2\mathbf{f}_x \partial_x + \mathbf{f} \partial_{xx} \end{bmatrix}, \\
A_{11} &= -\bar{\mathbf{u}} \Delta \partial_x - \bar{\mathbf{u}}_x \Delta - 2\bar{\mathbf{u}}_{xz} \partial_z - \bar{\mathbf{u}}_{zz} \partial_x - \bar{\mathbf{u}}_{zzz} + \frac{1}{Re} \Delta^2, \\
A_{12} &= -\bar{\mathbf{u}}_{zzz} + \bar{\mathbf{u}}_z \Delta + \bar{\mathbf{u}}_{xz} \partial_x - 2\bar{\mathbf{u}}_{zz} \partial_z, \\
A_{21} &= 2\bar{\mathbf{u}}_x \partial_{xz} + \bar{\mathbf{u}}_{xz} \partial_x + \bar{\mathbf{u}}_{xxz} + \bar{\mathbf{u}}_{xx} \partial_z, \\
A_{22} &= -\bar{\mathbf{u}}_{xx} \partial_x - \bar{\mathbf{u}}_x \Delta \partial_x - 2\bar{\mathbf{u}}_x \partial_{xx} + \bar{\mathbf{u}}_{zz} \partial_x - \bar{\mathbf{u}}_{zzz} + \frac{1}{Re} \Delta^2.
\end{aligned}$$

where,  $\mathbf{f}(x, z)$  in matrix  $B$  is a 2D shape function that determines the spatial extent of the forcing. For discretization of the domain and finite-dimensional approximation of the differential operators in the system matrices above, we use a second-order central differencing scheme with  $N_x$  and  $N_z$  uniformly distributed collocation points in the streamwise and spanwise directions, respectively. At the lateral edges of the computational domain, we enforce homogeneous Dirichlet and Neumann boundary conditions, i.e.,  $\mathbf{v}(x, z(1)) = \mathbf{v}(x, z(N_z)) = \mathbf{v}_x(x, z(1)) = \mathbf{v}_x(x, z(N_z)) = \mathbf{v}_z(x, z(1)) = \mathbf{v}_z(x, z(N_z)) = 0$ . At the inlet and outlet of the domain along the streamwise dimension, we apply linear extrapolation conditions

(see [79] for details), i.e.,

$$\begin{aligned}
\mathbf{v}(x(1), z) &= \alpha \mathbf{v}(x(2), z) + \beta \mathbf{v}(x(3), z), \\
\mathbf{v}(x(N_x), z) &= \alpha \mathbf{v}(x(N_x - 1), z) + \beta \mathbf{v}(x(N_x - 2), z), \\
\mathbf{v}_x(x(1), z) &= \alpha \mathbf{v}_x(x(2), z) + \beta \mathbf{v}_x(x(3), z), \\
\mathbf{v}_x(x(N_x), z) &= \alpha \mathbf{v}_x(x(N_x - 1), z) + \beta \mathbf{v}_x(x(N_x - 2), z), \\
\mathbf{v}_z(x(1), z) &= \alpha \mathbf{v}_z(x(2), z) + \beta \mathbf{v}_z(x(3), z), \\
\mathbf{v}_z(x(N_x), z) &= \alpha \mathbf{v}_z(x(N_x - 1), z) + \beta \mathbf{v}_z(x(N_x - 2), z)
\end{aligned}$$

where,

$$\alpha = \frac{x(N_x) - x(N_x - 2)}{x(N_x - 1) - x(N_x - 2)}, \quad \beta = \frac{x(N_x - 1) - x(N_x)}{x(N_x - 1) - x(N_x - 2)}.$$

Note that in the case of an equally spaced grid,  $\alpha = 2$  and  $\beta = -1$ . We also introduce sponge layers at the inflow and outflow to mitigate the influence of boundary conditions on the fluctuation dynamics within the computational domain [64, 73, 81].

#### 5.4 Thrust force and power predictions

The key quantities of interest in a wind farm are the thrust force and power. Thrust force informs about the kinetic energy that the turbine extracts from the wind and the power provides information about the energy output. Thus, accurate predictions of these quantities helps with optimizing the wind plant operation. As shown in Figures 3.1(c,d), the monotonically decreasing velocity field predicted by the analytical model  $\bar{\mathbf{u}}$  (5.2) fails to capture the increase in the thrust force and power after the second turbine in the cascade shown in Figure 3.1(a). The monotonic decrease in the flow energy can be attributed to the absence of a turbulence model that can promote turbulence in the near wake of turbines thereby energizing the velocity field and subsequently leading to higher thrust force and power generation in downstream turbines. This issue is particularly evident in the predictions of power generation for turbines located toward the end of the cascade (Figure 2.5(b)), indicating a deficiency that can only get worse in larger wind farms with more turbines. To improve predictions of wake recovery, we model the statistics of velocity fluctuations  $\mathbf{v}$  around  $\bar{\mathbf{u}}$  using the linearized NS equations subject to an optimally shaped source of additive stochastic excitation based on the the developments of Chapter 3.

Given a time-averaged thrust force measurement  $\bar{F}_i$  for the  $i$ th turbine segment, the effective flow intensity at the staggered point corresponding to that segment follows from equation (3.2a) as

$$\overline{\mathbf{v}}^2_{F,i} = \bar{F}_i / \left( \frac{1}{2} \rho A_i C_T \right) - \bar{\mathbf{u}}_{\text{eff},i}^2. \quad (5.3)$$

On the other hand, if instead we are provided with a time averaged power measurement  $\bar{P}_i$ , the effective flow intensity at the staggered point corresponding to that segment is given by

$$\overline{\mathbf{v}}^2_{P,i} = \left( \bar{P}_i / \left( \frac{1}{2} \rho A_i C_P \right) \right)^{2/3} - \bar{\mathbf{u}}_{\text{eff},i}^2. \quad (5.4)$$

Therefore, if thrust forces are provided, we may model the stochastic velocity field  $\mathbf{v}$  to match the effective intensity  $\overline{\mathbf{v}}^2_{F,i}$  and predict  $\bar{P}_i$ . Similarly, if power measurements are provided, we may model  $\mathbf{v}$  to match the effective intensity  $\overline{\mathbf{v}}^2_{P,i}$  in (5.4) and predict  $\bar{F}_i$ . However, due to a lack of sufficient degrees of freedom in Equations (3.2), both thrust force and power measurements cannot be simultaneously matched. To provide a balanced approximation of both, the velocity field  $\mathbf{v}$  can be modeled to match a balanced intensity  $\overline{\mathbf{v}}^2_{\text{bal}}$  per rotor segment as the solution to the problem:

$$\underset{\overline{\mathbf{v}}^2_{\text{bal},i} \geq 0}{\text{minimize}} \quad w_F |\overline{\mathbf{v}}^2_{\text{bal},i} - \overline{\mathbf{v}}^2_{F,i}| + w_P |\overline{\mathbf{v}}^2_{\text{bal},i} - \overline{\mathbf{v}}^2_{P,i}| \quad (5.5)$$

where weights  $w_F$  and  $w_P$  may be empirically determined to signify the importance of measurements over different turbine segments.

The velocity fluctuation field generated by the linearized NS equations augments the analytical wake model to improve predictions of thrust force and power generation based on the ADM model. Figure 5.1 demonstrates that whether we match thrust force or power generation predictions of the competing quantity also improve. This improvement, which also captures the non-monotonicity of such quantities over the turbines in the cascade, is also observed when we match a balanced approximation of the two quantities of interest based on the solution to problem (5.5) (Figure 5.1(c)). Importantly, the augmentation introduced to the predictions of the analytical model capture the non-monotonic trend of thrust force and power generation over the cascade of turbines. We anticipate this feature to be even more significant in larger arrays of wind turbines. Either way, we observe significantly improved predictions of the thrust force and power over the second, third, and fourth turbines while predictions at the first turbine depreciate. This is perhaps due to the fact that we model turbulence intensities at the turbine locations per thrust force and power measurements, but do not explicitly account for the statistical signature of the incoming turbulence impinging on the array.

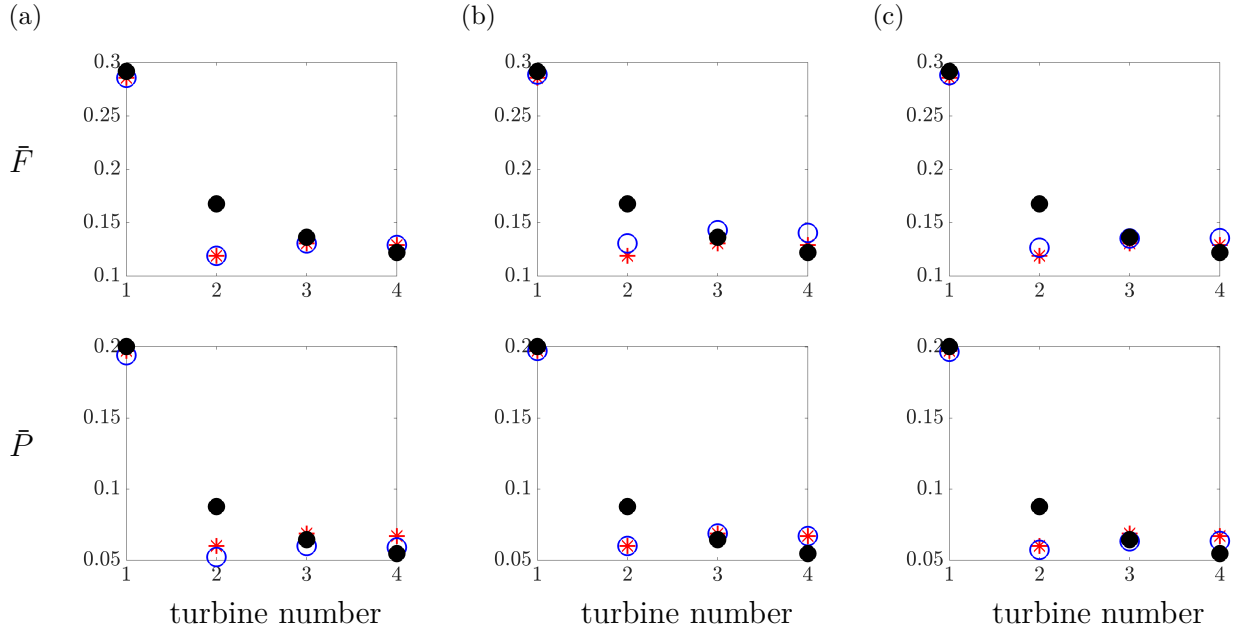


Figure 5.1: (a) Results for matching thrust force  $\bar{F}$  and predicting power generation  $\bar{P}$  over various turbines in the  $4 \times 1$  cascade; (b) Results for matching power generation  $\bar{P}$  and predicting thrust force  $\bar{F}$ ; (c) Results for matching the balanced approximation of both thrust force and power. LES data (\*); predictions of of analytical model [8] (●); and predictions of our data-enhanced stochastic dynamical model (○).

## 5.5 Turbulence intensity predictions

In this section, we evaluate the predictive capability of our stochastic modeling framework in completing the statistical signature of the hub-height turbulent velocity field for a single turbine as well as a 4-turbine cascade of turbines. Specifically, we will assume knowledge of the streamwise and spanwise turbulence intensities at various diameters behind wind turbines and predict the remainder of the second-order statistical signature of the flow using the stochastically forced linearized NS model (3.5). The available turbulence intensities may be provided by field measurement devices such as LiDAR systems that are deployed in wind farms to scan and monitor hub-height wind [46] or may represent effective velocity intensities over rotor structures obtained from power and thrust force measurements. The optimization framework of Section 4.1 identifies the appropriate colored-in-time forcing to the linearized NS equations to account for the available statistics and predict unavailable ones by virtue of the physics-based nature of model (3.5).



Figure 5.2: (a) Schematic of hub-height computational plane with data points used for training in Section 5.5.1 highlighted in red; (b) Hub-height streamwise velocity  $\bar{\mathbf{u}}(x, z)$  generated using the analytical wake-expansion model of Bastankhah and Porté-Agel [8] around which we linearize the NS equations.

### 5.5.1 Predicting the wake of a single turbine using partially available flow intensities

We first focus on the problem of predicting the streamwise  $uu$  and spanwise  $ww$  turbulence intensities at the hub height of single wind turbine. We consider a 2D computational domain of size  $L_x \times L_z = 5 \times 4$  where  $x \in [0, 5]$  and  $z \in [-2, 2]$ . The turbine of unit diameter is located at  $x = 2$  and  $z = 0$ . We use  $N_x = 13$  and  $N_z = 9$  equally spaced collocation points to discretize the computational domain rendering to the state in model (3.5)  $\mathbf{v} \in \mathbb{R}^{270 \times 1}$ . We use LES generated turbulent intensities at various locations within the computational domain to train our stochastic dynamical models. For consistency, we also use all data points before the turbine to match the inflow turbulence conditions with that of LES. We consider three cases in which the available training dataset contains 3 streams of streamwise and spanwise turbulent intensity measurements from behind the blade tips (edges of 2D rotor structure) and the turbine nacelle (middle of rotor structure) and at various distances away from the turbine: (i) at the turbine location  $x = 2$  and points within one diameter away (Figure 5.3(c) and 5.4(c)), (ii) at  $x = 2$  and points within 2 diameters away (Figures 5.3(e) and 5.4(e)), and (iii) at  $x = 2$  and points within 3 diameters away (Figures 5.3(g) and 5.4(g)). As evident from Figures 5.3(g) and 5.4(g), for the considered turbine and atmospheric conditions, access to flow statistics 3 diameters away from the turbine can significantly improve the completion of the statistical signature of the flow at hub height. Our results demonstrate the ability of the data-enhanced linearized NS equations in capturing the dominant trends of  $uu$  and  $ww$  in the wake of a turbine.

### 5.5.2 Predicting wind farm turbulence impinging on a cascade of turbines

We further extend our study to the case of a  $4 \times 1$  cascade of turbines that are aligned with the (streamwise) direction of the wind. We consider a similar 2D computational domain of size

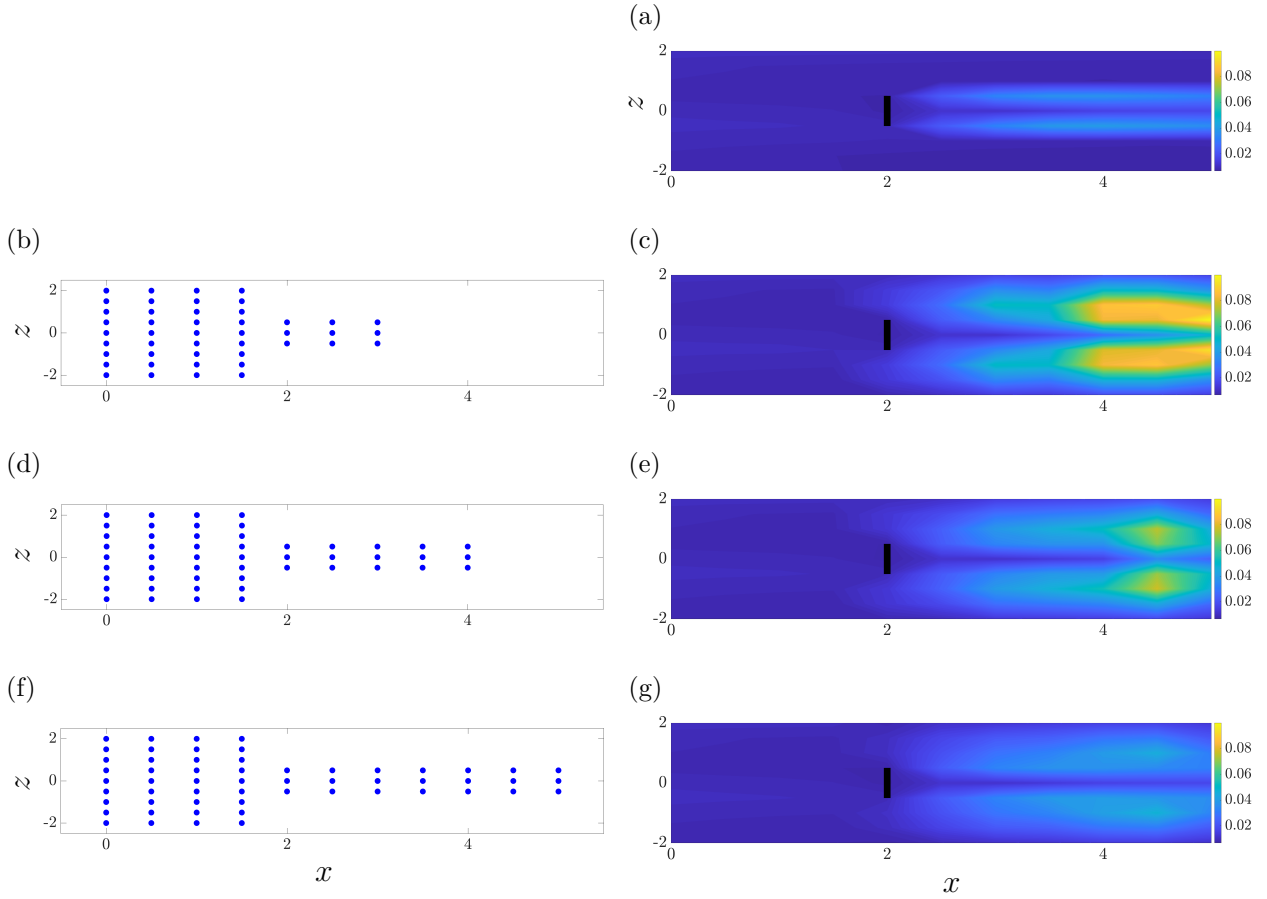


Figure 5.3: (a) Streamwise turbulence intensity ( $wu$ ) obtained from LES and (c,e,g) the results of our stochastic dynamical model with data provided at  $1d_0$  (c),  $2d_0$  (e), and  $3d_0$  (g) locations downstream of the turbine as shown by the blue dots in the figures on the left.

$L_x \times L_z = 16 \times 9$  where  $x \in [0, 16]$  and  $z \in [-2, 2]$ . Turbines of unit diameter are located at  $x = \{2, 6, 10, 14\}$  and  $z = 0$ . We use  $N_x = 38$  and  $N_z = 9$  equally spaced collocation points to discretize the computational domain rendering to the state in model (3.5)  $\mathbf{v} \in \mathbb{R}^{684 \times 1}$ . Given the findings of the single-turbine experiment, we use streamwise and spanwise intensities within 3 diameters behind the tips and nacelle of each of the turbines as data to train or stochastic models of the hub-height velocity field. Figure 5.5 demonstrates the performance of our data-enhanced stochastic model in predicting turbulence intensities at hub height. While the overall energy of the flow has been over-predicted by our model (as evident from the energetic patches throughout the farm), dominant features of the streamwise velocity correlations, including regions of high and low energy, are particularly well captured. The stochastic model is also shown to capture the spanwise asymmetry of flow intensities

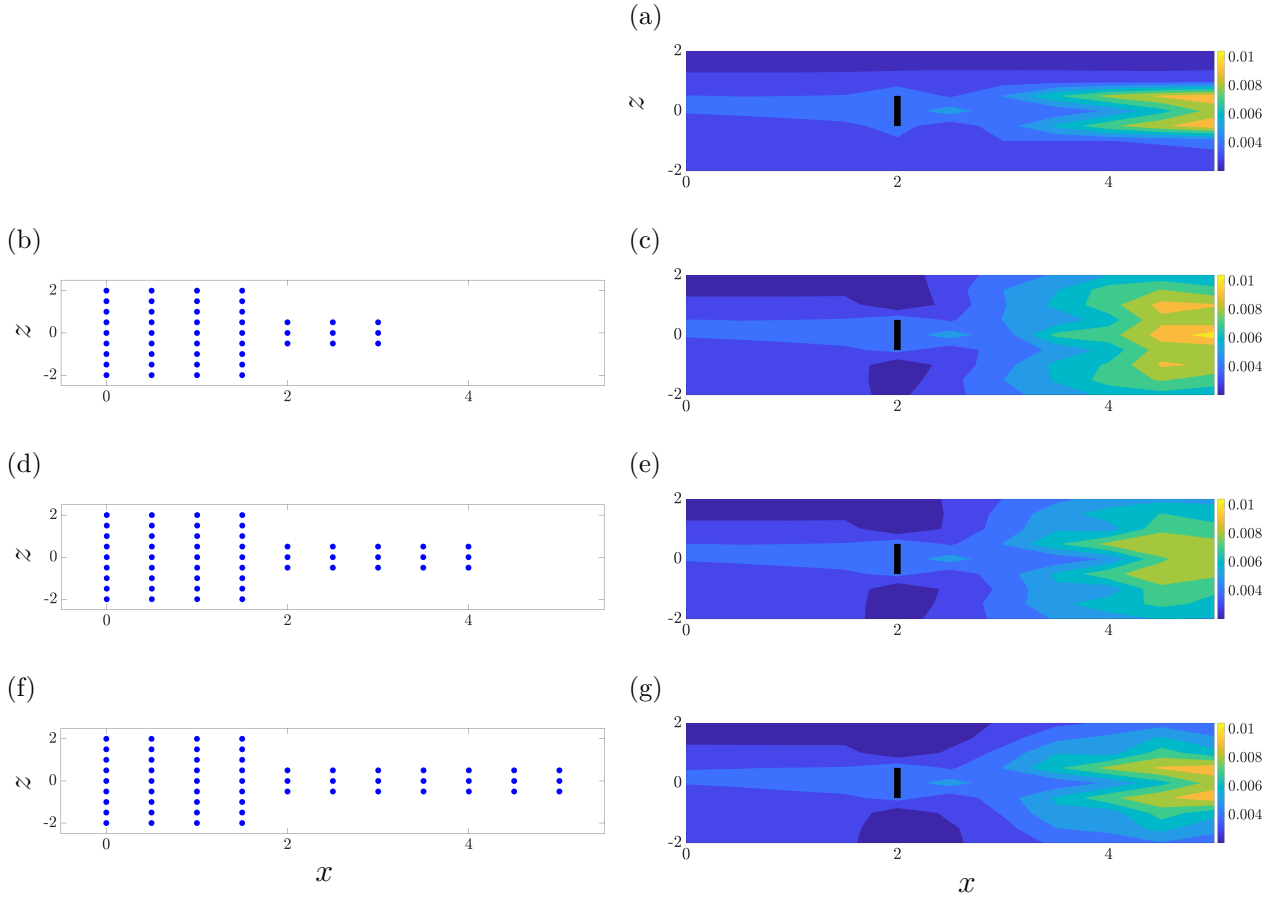


Figure 5.4: (a) Spanwise turbulence intensity ( $ww$ ) obtained from LES and (c,e,g) the results of our stochastic dynamical model with data provided at  $1d_0$  (c),  $2d_0$  (e), and  $3d_0$  (g) locations downstream of the turbine as shown by the blue dots in the figures on the left.

with respect to the centerline running through the turbine nacelles, which is attributed to the turbine’s rotation as captured by the high-fidelity LES (Figure 5.5(c)). Figure 5.5(d) shows that the high spanwise intensity regions behind the turbine nacelles are also captured very well by our models albeit spurious regions of high intensity appear in regions slightly beyond the the blade tips. Uncovering potential reasons behind such irregular predictions in the spanwise intensity calls for additional in-depth examination. Nevertheless, the good quality of completion shown in Figure 5.5 demonstrates the ability of our linear stochastic dynamical models in predicting the dominant statistical features of the flow and is attributed to the

Lyapunov-like constraint in covariance completion problem (4.1) [115, 112], which keeps physics in the mix and enforces consistency between data and the linearized NS dynamics.

In optimization problem 4.1, the regularization parameter  $\gamma$  determines the importance of the nuclear norm of matrix  $Z$  relative to the logarithmic barrier function of the covariance matrix  $X$ . Larger values of  $\gamma$  yield lower-rank matrices  $Z$ , but may compromise the quality of completion; see [115, Appendix C]. In this study,  $\gamma = 100$  was observed to provide the best quality of reproduction of the turbulence intensities of velocity fluctuations for both the single- and multi-turbine case studies. In training the stochastic model for the  $4 \times 1$  cascade of turbines (Figure 5.5), where  $N_x = 38$  and  $N_z = 9$  ( $Z$  is a square matrix of size 684),  $\gamma = 100$  results in the  $Z$  matrix that solves problem (4.1) having a rank of 266 with 265 positive and 1 negative eigenvalues. As discussed in Section (3.3), the presence of both positive and negative eigenvalues in matrix  $Z$  indicates that the second-order statistics of wind farm turbulence cannot be reproduced by the linearized NS equations with white-in-time stochastic excitation. The distribution of eigenvalues of matrix  $Z$  also indicates that 265 colored-in-time inputs are required to reproduce the partially available entries in covariance matrix  $X$  corresponding to the known velocity intensities; see Zare et al. [111, 115] for additional details.

## 5.6 Verification in stochastic linear simulations

As discussed in Section 4.2,  $Z$  can be decomposed into  $BH^* + HB^*$  with the input matrix  $B$  having 265 independent columns. In other words, the identified  $X$  can be explained by driving the LTI model (3.5) with 265 stochastic inputs  $d$ . The solution to the covariance completion problem (4.1) also determines the dynamics of the linear filter (4.2) that generates the coloured-in-time forcing  $d$  with appropriate power spectral density. We conduct stochastic linear simulations to verify our stochastic model of wind farm turbulence (Equation (3.5)). Since a proper comparison with LES requires ensemble averaging, rather than comparison at the level of individual stochastic simulations, we have conducted 20 simulations of system (3.5). The total simulation time was set to 300 time units. Figure 5.6 shows the time evolution of the energy (variance) of velocity fluctuations for 20 realizations of white-in-time forcing of the filter dynamics generating the colored-in-time input  $\mathbf{d}$  and exciting the linear dynamical model (3.5). The variance averaged over all simulations is marked by the thick black line, which asymptotically approaches the value of the total turbulent kinetic energy (averaged over space) in statistical steady state,  $\text{trace}(X)$ . For the above simulations the final average value has a 4.1% error in matching the training data provided by LES. This



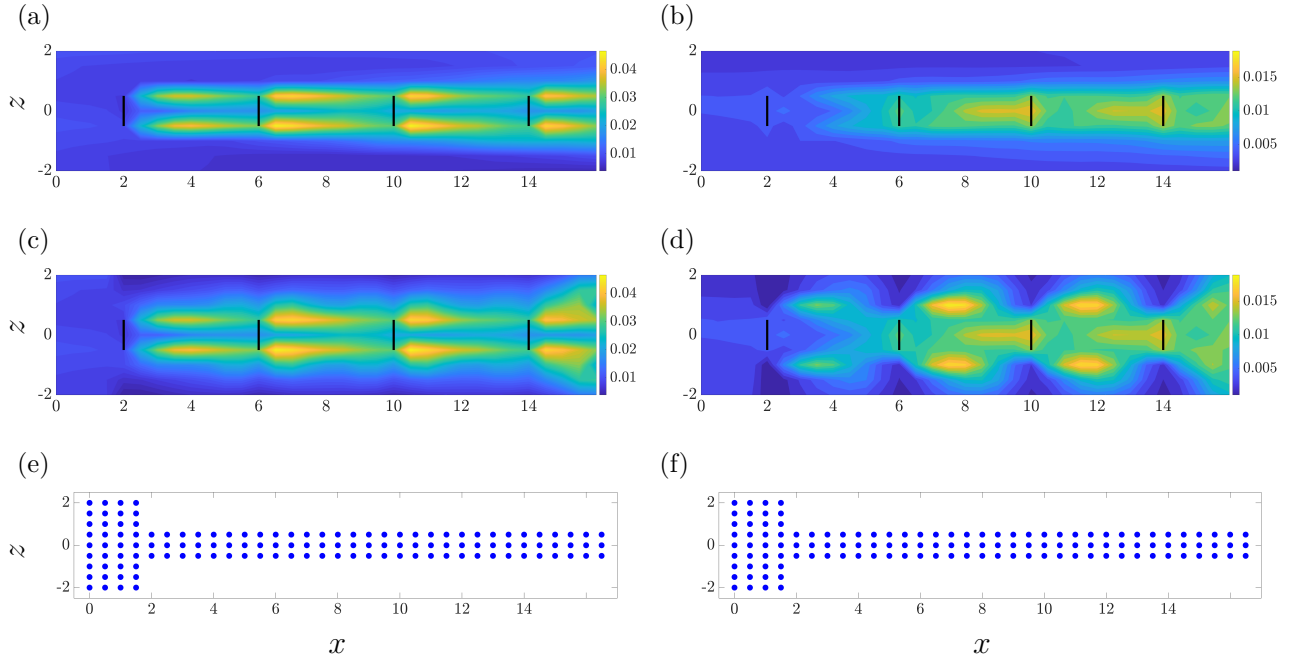


Figure 5.5: Streamwise  $uu$  (left) and spanwise  $ww$  (right) turbulence intensities resulting from LES (a,b) and our stochastic dynamical models (c,d) trained using all intermediate locations downstream of the turbine nacelle and blade tips shown by the blue dots in the plots on the last row.

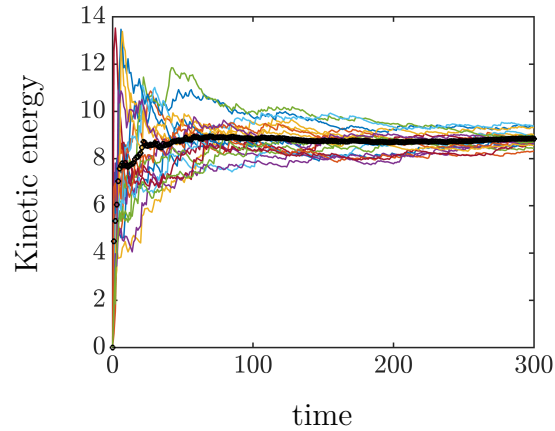


Figure 5.6: Time evolution of fluctuation kinetic energy for 20 realizations of the forcing to the modified linearized dynamics; the energy averaged over all simulations is marked by the thick black line.

close agreement can be further improved by running additional linear simulations and by increasing the total simulation times.

## CHAPTER 6

### CONCLUSIONS AND FUTURE DIRECTIONS

#### 6.1 Conclusions

We provide a framework for the stochastic dynamical modeling of wind farm turbulence with enhanced predictive capability relative to conventional low-fidelity models that provide a static (albeit analytical) description of turbine wakes. We focus on the estimation of quantities that are pertinent to control, i.e., thrust forces, power generation, and turbulence intensities throughout wind farms. To capture the complex dynamical nature of wake turbulence, our proposed approach uses experimentally or numerically generated wind farm quantities to train data-enhanced physics-based models of flow fluctuations that match the available data and complete the statistical signature of the flow. We leverage the predictive capability of the linearized NS equations subject to judiciously shaped additive stochastic excitation as a physics-based model that can overcome potential robustness issues of solely data-driven models in the presence of highly variable atmospheric turbulence. The low-complexity and dynamic nature of this class of models is particularly desirable in handling varying atmospheric conditions that may necessitate online parametric updates based on SCADA measurements. The characteristic features of our models that render them desirable for estimation and control are their: (i) physics-based dynamic nature; (ii) linearity; (iii) low computational complexity; and (iv) statistical consistency in matching flow quantities that are of interest in flow analysis and control.

We utilize time-averaged LES-generated measurements of thrust forces and/or power generation in addition to turbulence intensities to identify stochastic realizations of forcing into linear approximations of the turbulent flow dynamics to achieve consistency in matching statistical quantities of interest. To demonstrate the utility of our approach, we use the stochastically forced linearized NS equations around a 2D static velocity profile of a wind farm consisting of a cascade of 4 turbine and show that stochastic modeling of input forcing allows us to significantly improve the predictions of low-fidelity analytical models. We provide details on how matching thrust force (power generation) measurements across various turbines can lead to improved predictions of power generation (thrust force). We also demonstrate the value of turbulent intensity measurements at various distances behind wind turbines in completing the statistical signature of hub-height turbulence, which include dominant features of the velocity correlations and regions of high and low turbulence. We verify our stochastic dynamical models using inexpensive stochastic linear simulations



Figure 6.1: Our proposed modeling approach which uses data to augment the low-fidelity model using a stochastic dynamical representation thus, providing improvements to their predictive capabilities.

that also highlight the ease of using our low-complexity models for generating statistically consistent turbulent inflow conditions for numerical simulations.

## 6.2 Future Directions

The proposed framework allows for linearization around more complicated (potentially 3D) base flow profiles that can better represent the effects of turbine yawing (e.g., wake curl and deflection) [83] or alternative turbine arrangements within a wind farm. Development of 3D extensions of the model that resolve the velocity field down to surface and can enable ground sensing capabilities in wind farms, the use such models for sequential data-assimilation, e.g., Kalman filtering, with applications to real-time wind forecasting, and the use of alternative covariance completion formulations [116] that may provide useful information about critical directions that have maximal effect in bringing model (in our case the stochastically forced linearized NS) and statistics in agreement. Given the physics-based nature of our models, the latter research direction can prove critical in identifying salient dynamical couplings and interactions in turbine wakes thereby opening the door to new classes of low-fidelity wake models.

## REFERENCES

- [1] Abramovich, G. (1963). *The theory of turbulent jets*. MIT Press, Cambridge, Mass.
- [2] Ahmad, T., A. Basit, M. Ahsan, O. Coupiac, N. Girard, B. Kazemtabrizi, and P. C. Matthews (2019). Implementation and analyses of yaw based coordinated control of wind farms. *Energies* 12(7), 1266.
- [3] Ainslie, J. F. (1988). Calculating the flowfield in the wake of wind turbines. *J. Wind Eng. Ind. Aerodyn.* 27(1-3), 213–224.
- [4] Annoni, J., K. Howard, P. Seiler, and M. Guala (2016). An experimental investigation on the effect of individual turbine control on wind farm dynamics. *Wind Energy* 19(8), 1453–1467.
- [5] Annoni, J. R., J. Nichols, and P. J. Seiler (2016). Wind farm modeling and control using dynamic mode decomposition. In *34th Wind Energy Symposium*, pp. 2201. Wind Energy Symposium.
- [6] Bamieh, B. and M. Dahleh (2001). Energy amplification in channel flows with stochastic excitation. *Phys. Fluids* 13(11), 3258–3269.
- [7] Barthelmie, R., S. T. Frandsen, K. Hansen, J. Schepers, K. Rados, W. Schlez, A. Neubert, L. E. Jensen, and S. Neckelmann (2009). Modelling the impact of wakes on power output at Nysted and Horns Rev. In *European Wind Energy Conference*, pp. 1–10.
- [8] Bastankhah, M. and F. Porté-Agel (2014). A new analytical model for wind-turbine wakes. *Renewable energy* 70, 116–123.
- [9] Bastankhah, M., C. R. Shapiro, S. Shamsoddin, D. F. Gayme, and C. Meneveau (2022). A vortex sheet based analytical model of the curled wake behind yawed wind turbines. *J. Fluid Mech.* 933.
- [10] Boersma, S., B. Doekemeijer, M. Vali, J. Meyers, and J.-W. van Wingerden (2018). A control-oriented dynamic wind farm model: WFSim. *Wind Energy Sci.* 3(1), 75–95.
- [11] Boersma, S., M. Vali, M. Kühn, and J.-W. van Wingerden (2016). Quasi linear parameter varying modeling for wind farm control using the 2D Navier-Stokes equations. In *2016 American Control Conference (ACC)*, pp. 4409–4414. IEEE.
- [12] Bossanyi, E. A. and R. Ruisi (2020). Axial induction controller field test at sedini wind farm. *Wind Energy Sci. Discussions* 2020, 1–27.
- [13] Boyd, S. and L. Vandenberghe (2004). *Convex optimization*. Cambridge University Press.

- [14] Burton, T., N. Jenkins, D. Sharpe, and E. Bossanyi (2011). *Wind energy handbook*. John Wiley & Sons.
- [15] Butler, K. M. and B. F. Farrell (1992). Three-dimensional optimal perturbations in viscous shear flow. *Phys. Fluids A* 4, 1637.
- [16] Campagnolo, F., A. Molder, J. Schreiber, and C. Bottasso (2019). Comparison of analytical wake models with wind tunnel data. In *J. Phys. Conf. Ser.*, Volume 1256, pp. 012006. IOP Publishing.
- [17] Chevalier, M., J. Höpfner, T. R. Bewley, and D. S. Henningson (2006). State estimation in wall-bounded flow systems. Part 2. Turbulent flows. *J. Fluid Mech.* 552, 167–187.
- [18] Ciri, U., G. Petrolo, M. V. Salvetti, and S. Leonardi (2017). Large-eddy simulations of two in-line turbines in a wind tunnel with different inflow conditions. *Energies* 10(6), 821.
- [19] Ciri, U., M. A. Rotea, and S. Leonardi (2017). Model-free control of wind farms: A comparative study between individual and coordinated extremum seeking. *Renewable energy* 113, 1033–1045.
- [20] Ciri, U., M. Salvetti, K. Carrasquillo, C. Santoni, G. Iungo, and S. Leonardi (2018). Effects of the subgrid-scale modeling in the large-eddy simulations of wind turbines. In *Direct and Large-Eddy Simulation X*, pp. 109–115. Springer.
- [21] Creaby, J., Y. Li, and J. E. Seem (2009). Maximizing wind turbine energy capture using multivariable extremum seeking control. *Wind Engineering* 33(4), 361–387.
- [22] Del Álamo, J. C. and J. Jiménez (2003). Spectra of the very large anisotropic scales in turbulent channels. *Phys. Fluids* 15(6), 41–44.
- [23] Del Álamo, J. C., J. Jiménez, P. Zandonade, and R. D. Moser (2004). Scaling of the energy spectra of turbulent channels. *J. Fluid Mech.* 500(1), 135–144.
- [24] Doekemeijer, B. M., S. Kern, S. Maturu, S. Kanev, B. Salbert, J. Schreiber, F. Campagnolo, C. L. Bottasso, S. Schuler, F. Wilts, et al. (2021). Field experiment for open-loop yaw-based wake steering at a commercial onshore wind farm in italy. *Wind Energy Sci.* 6(1), 159–176.
- [25] Doekemeijer, B. M., D. van der Hoek, and J.-W. van Wingerden (2020). Closed-loop model-based wind farm control using FLORIS under time-varying inflow conditions. *Renew. Energy* 156, 719–730.

- [26] Doekemeijer, B. M., J.-W. van Wingerden, and P. A. Fleming (2019). A tutorial on the synthesis and validation of a closed-loop wind farm controller using a steady-state surrogate model. In *2019 American Control Conference (ACC)*, pp. 2825–2836. IEEE.
- [27] Duc, T., O. Coupiac, N. Girard, G. Giebel, and T. Göçmen (2019). Local turbulence parameterization improves the jensen wake model and its implementation for power optimization of an operating wind farm. *Wind Energy Sci.* 4(2), 287–302.
- [28] Farrell, B. F. and P. J. Ioannou (1993). Stochastic forcing of the linearized Navier-Stokes equations. *Phys. Fluids A* 5(11), 2600–2609.
- [29] Fazel, M. (2002). *Matrix rank minimization with applications*. Ph. D. thesis, Stanford University.
- [30] Fleming, P., J. Annoni, J. J. Shah, L. Wan, S. Ananthan, Z. Zhang, K. Hutchings, P. Wang, W. Chen, and L. Chen (2017). Field test of wake steering at an offshore wind farm. *Wind Energy Sci.* 2(1), 229–239.
- [31] Fleming, P., J. King, E. Simley, J. Roadman, A. Scholbrock, P. Murphy, J. K. Lundquist, P. Moriarty, K. Fleming, J. van Dam, et al. (2020). Continued results from a field campaign of wake steering applied at a commercial wind farm—part 2. *Wind Energy Sci.* 5(3), 945–958.
- [32] Frandsen, S., R. Barthelmie, S. Pryor, O. Rathmann, S. Larsen, J. Højstrup, and M. Thøgersen (2006). Analytical modelling of wind speed deficit in large offshore wind farms. *Wind Energy: An International Journal for Progress and Applications in Wind Power Conversion Technology* 9(1-2), 39–53.
- [33] Gebraad, P. M. O. and J. W. van Wingerden (2014). A control-oriented dynamic model for wakes in wind plants. In *J. Phys. Conf. Ser.*, Volume 524, pp. 012186.
- [34] Georgiou, T. T. (2002a). Spectral analysis based on the state covariance: the maximum entropy spectrum and linear fractional parametrization. *IEEE Trans. Autom. Control* 47(11), 1811–1823.
- [35] Georgiou, T. T. (2002b). The structure of state covariances and its relation to the power spectrum of the input. *IEEE Trans. Autom. Control* 47(7), 1056–1066.
- [36] Goit, J. P. and J. Meyers (2015). Optimal control of energy extraction in wind-farm boundary layers. *J. Fluid Mech.* 768, 5–50.
- [37] Goit, J. P., W. Munters, and J. Meyers (2016). Optimal coordinated control of power extraction in les of a wind farm with entrance effects. *Energies* 9(1), 29.
- [38] Grant, M. and S. Boyd (2014, March). CVX: Matlab Software for Disciplined Convex Programming, version 2.1. <http://cvxr.com/cvx>.

- [39] Guo, Y., M. Rotea, and T. Summers (2020). Stochastic dynamic programming for wind farm power maximization. In *2020 American Control Conference (ACC)*, pp. 4824–4829. IEEE.
- [40] Hannah, R., R. Max, and R. Pablo (2022). Energy. <https://ourworldindata.org/energy>.
- [41] Hoepffner, J., M. Chevalier, T. R. Bewley, and D. S. Henningson (2005). State estimation in wall-bounded flow systems. Part 1. Perturbed laminar flows. *J. Fluid Mech.* *534*, 263–294.
- [42] Howland, M. F., K. S. Lele, and J. O. Dabiri (2019). Wind farm power optimization through wake steering. *Proc. Natl. Acad. Sci.* *116*(29), 14495–14500.
- [43] Hutchins, N., J. P. Monty, B. Ganapathisubramani, H. C.-H. Ng, and I. Marusic (2011). Three-dimensional conditional structure of a high-Reynolds-number turbulent boundary layer. *J. Fluid Mech.* *673*, 255–285.
- [44] Hwang, Y. and C. Cossu (2010). Linear non-normal energy amplification of harmonic and stochastic forcing in the turbulent channel flow. *J. Fluid Mech.* *664*, 51–73.
- [45] Iungo, G. V., F. Viola, U. Ciri, S. Leonardi, and M. Rotea (2016). Reduced order model for optimization of power production from a wind farm. In *34th Wind Energy Symposium*, pp. 2200. Wind Energy Symposium.
- [46] Iungo, G. V., Y.-T. Wu, and F. Porté-Agel (2013). Field measurements of wind turbine wakes with lidars. *J. Atmos. Ocean. Technol.* *30*(2), 274–287.
- [47] J. Annoni, P. G. and P. Seiler (2016). Wind farm flow modeling using an input-output reduced-order model. In *2016 American Control Conference (ACC)*, pp. 506–512. IEEE.
- [48] Jensen, N. O. (1983). A note on wind generator interaction. *Roskilde, Denmark: Risø National Laboratory*.
- [49] Johnson, K. E. and G. Fritsch (2012). Assessment of extremum seeking control for wind farm energy production. *Wind Engineering* *36*(6), 701–715.
- [50] Johnson, K. E., L. Y. Pao, M. J. Balas, and L. J. Fingersh (2006). Control of variable-speed wind turbines: standard and adaptive techniques for maximizing energy capture. *IEEE Control Systems Magazine* *26*(3), 70–81.
- [51] Jonkman, J., S. Butterfield, W. Musia, and G. Scott (2009). Definition of a 5-MW reference wind turbine for offshore system development. Technical report, National Renewable Energy Lab. (NREL), Golden, CO, USA.

- [52] Jonkman, J., S. Butterfield, W. Musial, and G. Scott (2009). Definition of a 5-mw Reference Wind Turbine for Offshore System Development. Technical Report NREL/TP-500-38060, NREL - National Renewable Energy Laboratory, Golden, Co, USA.
- [53] Jovanovic, M. R. (2004). *Modeling, analysis, and control of spatially distributed systems*. Ph. D. thesis, University of California, Santa Barbara.
- [54] Jovanovic, M. R. (2008, January). Turbulence suppression in channel flows by small amplitude transverse wall oscillations. *Phys. Fluids* 20(1), 014101 (11 pages).
- [55] Jovanovic, M. R. and B. Bamieh (2005, July). Componentwise energy amplification in channel flows. *J. Fluid Mech.* 534, 145–183.
- [56] Jovanovic, M. R., P. J. Schmid, and J. W. Nichols (2014, February). Sparsity-promoting dynamic mode decomposition. *Phys. Fluids* 26(2), 024103 (22 pages).
- [57] Katic, I., J. Højstrup, and N. O. Jensen (1986). A simple model for cluster efficiency. In *European wind energy association conference and exhibition*, Volume 1, pp. 407–410. Rome, Italy.
- [58] Khadra, K., P. Angot, S. Parneix, and J. Caltagirone (2000). Fictitious domain approach for numerical modelling of Navier-Stokes equations. *Int. J. Numer. Methods Fluids* 34(8), 651–684.
- [59] Laks, J. H., L. Y. Pao, and A. D. Wright (2009). Control of wind turbines: Past, present, and future. In *2009 American Control Conference (ACC)*, pp. 2096–2103. IEEE.
- [60] Larsen, G. C., H. A. Madsen, K. Thomsen, and T. J. Larsen (2008). Wake meandering: a pragmatic approach. *Wind Energy* 11(4), 377–395.
- [61] Leonardi, S. and I. P. Castro (2010). Channel flow over large cube roughness: a direct numerical simulation study. *Journal of Fluid Mechanics* 651, 519–539.
- [62] Letizia, S. and G. V. Iungo (2022). Pseudo-2D RANS: A LiDAR-driven mid-fidelity model for simulations of wind farm flows. *J. Renew. Sustain. Energy* 14(2), 023301.
- [63] Lissaman, P. B. S. (1979). Energy effectiveness of arbitrary arrays of wind turbines. *Journal of Energy* 3(6), 323–328.
- [64] Mani, A. (2012). Analysis and optimization of numerical sponge layers as a nonreflective boundary treatment. *J. Comput. Phys.* 231(2), 704–716.
- [65] Martínez-Tossas, L. A., J. Annoni, P. A. Fleming, and M. J. Churchfield (2019). The aerodynamics of the curled wake: a simplified model in view of flow control. *Wind Energy Sci.* 4(1), 127–138.



- [66] Martínez-Tossas, L. A. and E. Branlard (2020). The curled wake model: equivalence of shed vorticity models. In *J. Phys. Conf. Ser.*, Volume 1452, pp. 012069. IOP Publishing.
- [67] McKeon, B. J. and A. S. Sharma (2010). A critical-layer framework for turbulent pipe flow. *J. Fluid Mech.* 658, 336–382.
- [68] Moarref, R. and M. R. Jovanovic (2010, November). Controlling the onset of turbulence by streamwise traveling waves. part 1: Receptivity analysis. *J. Fluid Mech.* 663, 70–99.
- [69] Moarref, R. and M. R. Jovanovic (2012, September). Model-based design of transverse wall oscillations for turbulent drag reduction. *J. Fluid Mech.* 707, 205–240.
- [70] Munters, W. and J. Meyers (2017). An optimal control framework for dynamic induction control of wind farms and their interaction with the atmospheric boundary layer. *Philosophical Transactions of the Royal Society A: Mathematical, Physical and Engineering Sciences* 375(2091), 20160100.
- [71] Munters, W. and J. Meyers (2018a). Dynamic strategies for yaw and induction control of wind farms based on large-eddy simulation and optimization. *Energies* 11(1), 177.
- [72] Munters, W. and J. Meyers (2018b). Towards practical dynamic induction control of wind farms: analysis of optimally controlled wind-farm boundary layers and sinusoidal induction control of first-row turbines. *Wind Energy Sci.* 3(1), 409–425.
- [73] Nichols, J. W. and S. K. Lele (2011). Global modes and transient response of a cold supersonic jet. *J. Fluid Mech.* 669, 225–241.
- [74] Noack, B. R., M. Morzyński, and G. Tadmor (2011). *Reduced-order modelling for flow control*, Volume 528 of *CISM Courses and Lectures*. Springer.
- [75] Orlandi, P. and S. Leonardi (2006). Dns of turbulent channel flows with two- and three-dimensional roughness. *J. Turbul.* 7, 1–22.
- [76] Orlandi, I. (1976). A simple boundary condition for unbounded hyperbolic flows. *Journal of computational physics* 21(3), 251–269.
- [77] Porté-Agel, F., M. Bastankhah, and S. Shamsoddin (2020). Wind-turbine and wind-farm flows: a review. *Bound.-Layer Meteorol.* 174(1), 1–59.
- [78] Porté-Agel, F., H. Lu, and Y.-T. Wu (2010). A large-eddy simulation framework for wind energy applications. In *The Fifth International Symposium on Computational Wind Engineering*, Volume 23, pp. 27. Chapel Hill North Carolina.
- [79] Ran, W., A. Zare, M. J. P. Hack, and M. R. Jovanovic (2019, September). Stochastic receptivity analysis of boundary layer flow. *Phys. Rev. Fluids* 4(9), 093901 (28 pages).

- [80] Ran, W., A. Zare, and M. R. Jovanović (2021, January). Model-based design of riblets for turbulent drag reduction. *J. Fluid Mech.* 906, A7 (38 pages).
- [81] Ran, W., A. Zare, J. W. Nichols, and M. R. Jovanovic (2017). The effect of sponge layers on global stability analysis of blasius boundary layer flow. In *Proceedings of the 47th AIAA Fluid Dynamics Conference*, Denver, CO, pp. 3456 (12 pages). AIAA Fluid Dynamics Conference.
- [82] Recht, B., M. Fazel, and P. A. Parrilo (2010). Guaranteed minimum-rank solutions of linear matrix equations via nuclear norm minimization. *SIAM Rev.* 52(3), 471–501.
- [83] Rodrigues, M., N. A. Burgess, A. H. Bhatt, S. Leonardi, and A. Zare (2023). Robustness of two-dimensional stochastic dynamical wake models for yawed wind turbines. In *Proceedings of the 2023 American Control Conference*. Submitted.
- [84] S. Raach, D. S. and P. W. Cheng (2017). Lidar-based wake tracking for closed-loop wind farm control. *Wind Energy Sci.* 2(1), 257–267.
- [85] Santoni, C., K. Carrasquillo, I. Arenas-Navarro, and S. Leonardi (2017a). Effect of tower and nacelle on the flow past a wind turbine. *Wind Energy* 20(12), 1927–1939.
- [86] Santoni, C., K. Carrasquillo, I. Arenas-Navarro, and S. Leonardi (2017b). Effect of tower and nacelle on the flow past a wind turbine. *Wind Energy* 20(12), 1927–1939.
- [87] Santoni, C., U. Ciri, M. Rotea, and S. Leonardi (2015). Development of a high fidelity cfd code for wind farm control. In *2015 American Control Conference (ACC)*, pp. 1715–1720. IEEE.
- [88] Santoni, C., E. J. García-Cartagena, U. Ciri, L. Zhan, G. V. Iungo, and S. Leonardi (2020). One-way mesoscale-microscale coupling for simulating a wind farm in North Texas: Assessment against SCADA and LiDAR data. *Wind Energy* 23(3), 691–710.
- [89] Schmid, P. J. (2010). Dynamic mode decomposition of numerical and experimental data. *J. Fluid Mech.* 656, 5–28.
- [90] Schmid, P. J. (2022). Dynamic mode decomposition and its variants. *Annu. Rev. Fluid Mech.* 54, 225–254.
- [91] Schultz, M. P. and K. A. Flack (2013). Reynolds-number scaling of turbulent channel flow. *Phys. Fluids* 25, 025104.
- [92] Sillero, J. A., J. Jiménez, and R. D. Moser (2013). One-point statistics for turbulent wall-bounded flows at Reynolds numbers up to  $\delta^+ \approx 2000$ . *Phys. Fluids* 25, 105102.

- [93] Sillero, J. A., J. Jiménez, and R. D. Moser (2014). Two-point statistics for turbulent boundary layers and channels at Reynolds numbers up to  $\delta^+ \approx 2000$ . *Phys. Fluids* 26, 105109.
- [94] Simley, E., P. Fleming, N. Girard, L. Alloin, E. Godefroy, and T. Duc (2021). Results from a wake-steering experiment at a commercial wind plant: investigating the wind speed dependence of wake-steering performance. *Wind Energy Sci.* 6(6), 1427–1453.
- [95] Singh, P. and P. Seiler (2019). Controlling the meandering wake using measurement feedback. In *2019 American Control Conference (ACC)*, pp. 4144–4150. IEEE.
- [96] Sinner, M., L. Y. Pao, and J. King (2020). Estimation of large-scale wind field characteristics using supervisory control and data acquisition measurements. In *2020 American Control Conference (ACC)*, pp. 2357–2362. IEEE.
- [97] Skogestad, S. and I. Postlethwaite (2007). *Multivariable feedback control: analysis and design*, Volume 2. Wiley New York.
- [98] Soleimanzadeh, M., R. Wisniewski, and A. Brand (2014). State-space representation of the wind flow model in wind farms. *Wind Energy* 17(4), 627–639.
- [99] Stevens, R. J. A. M. and C. Meneveau (2017). Flow structure and turbulence in wind farms. *Annu. Rev. Fluid Mech* 49(1), 311–339.
- [100] Stull, R. B. (1988). *An introduction to boundary layer meteorology*, Volume 13. Springer Science & Business Media.
- [101] Tadmor, G. and B. R. Noack (2011). Bernoulli, Bode, and Budgie [Ask the Experts]. *IEEE Contr. Syst. Mag.* 31(2), 18–23.
- [102] Toh, K.-C., M. J. Todd, and R. H. Tütüncü (1999). SDPT3 — a MATLAB software package for semidefinite programming, version 1.3. *Optimization methods and software* 11(1-4), 545–581.
- [103] Trefethen, L. N., A. E. Trefethen, S. C. Reddy, and T. A. Driscoll (1993). Hydrodynamic stability without eigenvalues. *Science* 261, 578–584.
- [104] UN. World Population Prospects 2022. <https://population.un.org/wpp/Graphs/Probabilistic/POP/TOT/900>.
- [105] van Kuik, G. A. M., J. Peinke, R. Nijssen, D. Lekou, J. Mann, J. N. Sørensen, C. Ferreira, J. W. van Wingerden, D. Schlipf, P. Gebraad, H. Polinder, A. Abrahamsen, G. J. W. van Bussel, J. D. Sørensen, P. Tavner, C. L. Bottasso, M. Muskulus, D. Matha, H. J. Lindeboom, S. Degraer, O. Kramer, S. Lehnhoff, M. Sonnenschein, P. E. Sørensen, R. W. Kanneke, P. E. Morthorst, and K. Skytte (2016). Long-term research challenges in wind energy—a research agenda by the European Academy of Wind Energy. *Wind Energy Sci.* 1(1), 1–39.

- [106] Veers, P., K. Dykes, E. Lantz, S. Barth, C. L. Bottasso, O. Carlson, A. Clifton, J. Green, P. Green, H. Holttinen, et al. (2019). Grand challenges in the science of wind energy. *Science* 366(6464).
- [107] VerdeEnergyUSA. Which energy is more efficient solar or wind energy? <https://www.verdeenergy.com/>.
- [108] VerHulst, C. and C. Meneveau (2014). Large eddy simulation study of the kinetic energy entrainment by energetic turbulent flow structures in large wind farms. *Phys. Fluids* 26, 025113.
- [109] Wang, L., A. C. Tan, M. Cholette, and Y. Gu (2016). Comparison of the effectiveness of analytical wake models for wind farm with constant and variable hub heights. *Energy Conversion and Management* 124, 189–202.
- [110] Wu, Y.-T. and F. Porté-Agel (2011). Large-eddy simulation of wind-turbine wakes: evaluation of turbine parametrisations. *Bound.-Layer Meteorol.* 138(3), 345–366.
- [111] Zare, A., Y. Chen, M. R. Jovanovic, and T. T. Georgiou (2017, March). Low-complexity modeling of partially available second-order statistics: theory and an efficient matrix completion algorithm. *IEEE Trans. Automat. Control* 62(3), 1368–1383.
- [112] Zare, A., T. T. Georgiou, and M. R. Jovanovic (2020, May). Stochastic dynamical modeling of turbulent flows. *Annu. Rev. Control Robot. Auton. Syst.* 3, 195–219.
- [113] Zare, A., M. R. Jovanovic, and T. T. Georgiou (2015). Alternating direction optimization algorithms for covariance completion problems. In *Proceedings of the 2015 American Control Conference*, Chicago, IL, pp. 515–520.
- [114] Zare, A., M. R. Jovanovic, and T. T. Georgiou (2016). Perturbation of system dynamics and the covariance completion problem. In *Proceedings of the 55th IEEE Conference on Decision and Control*, pp. 7036–7041. IEEE.
- [115] Zare, A., M. R. Jovanovic, and T. T. Georgiou (2017, February). Colour of turbulence. *J. Fluid Mech.* 812, 636–680.
- [116] Zare, A., H. Mohammadi, N. K. Dhingra, T. T. Georgiou, and M. R. Jovanović (2020, August). Proximal algorithms for large-scale statistical modeling and sensor/actuator selection. *IEEE Trans. Automat. Control* 65(8), 3441–3456.
- [117] Zhan, L., S. Letizia, and G. Iungo (2020). Optimal tuning of engineering wake models through lidar measurements. *Wind Energy Sci.* 5(4), 1601–1622.
- [118] Zho, K. and J. C. Doyle (1998). *Essentials of robust control*, Volume 104. Prentice hall Upper Saddle River, NJ.
- [119] Zong, H. and F. Porté-Agel (2020). A point vortex transportation model for yawed wind turbine wakes. *J. Fluid Mech* 890.

## **BIOGRAPHICAL SKETCH**

Aditya H. Bhatt was born and raised in India. He earned his BE degree in mechanical engineering from Mumbai University in 2019. Owing to his passion for automobiles, during his under graduate studies he actively participated in Formula Student activities from 2016 to 2019. He began his master's studies in Mechanical Engineering at The University of Texas at Dallas in 2021. Under the supervision of Dr. Armin Zare he has worked on development of low fidelity models implementing stochastic dynamical modeling framework for wind farms.

# CURRICULUM VITAE

## Aditya H Bhatt

### EDUCATION

---

<b>MS in Mechanical Engineering</b> <i>The University of Texas at Dallas, Dallas, TX</i> Advisor: Professor Armin Zare	Dec 2022
<b>BE in Mechanical Engineering</b> <i>Mumbai University, Mumbai, IN</i>	May 2019

### SKILLS

---

<b>Tools and Languages</b>	Matlab & Simulink, Adams, Python, C++, Git, LaTeX
<b>Operating Systems</b>	MacOS, Windows
<b>CAD/CAE</b>	Solidworks (Certified), Creo, Ansys Workbench
<b>Communication</b>	English, German (B2 Niveau), Hindi, Gujarati (Native)

### ACADEMIC PROJECTS

---

<b>Stochastic Wake Modeling</b>	Jan 2021 — Present
<ul style="list-style-type: none"><li>Working with Dr. Armin Zare, developing a control oriented low complexity linear wake model for wind turbines in a wind farm to increase energy output. The model leverages physics involved in fluid flows to model stochastic forcing that reproduces the second order statistics of turbulent flows in the wind farm.</li></ul>	
<b>Model Predictive Control - Driver Model</b>	Aug 2021 — Dec 2021
<ul style="list-style-type: none"><li>Developed a model predictive controller based on the bicycle model dynamics to implement a lane changing scenario. The controller solved non-linear optimization problem to identify optimal input for the bicycle model.</li></ul>	
<b>Vehicle Modeling in Simulink</b>	Aug 2018 — May 2019
<ul style="list-style-type: none"><li>Using first principles, modeled suspension, brakes, steering responses of a vehicle.</li><li>Utilizing control feedback, simulated the performance of vehicle around a track, and made setup changes based on the results to improve on-track performance of the car.</li></ul>	
<b>Formula SAE Tire Modeling</b>	Jan 2018 — May 2018
<ul style="list-style-type: none"><li>Implemented the Pacejka tire model for FSAE tires. The model was used to compare real-world data obtained using the accelerometers and gyroscope on a FSAE vehicle.</li></ul>	

### PUBLICATIONS & ABSTRACTS

---

- A. H. Bhatt, F. Bernardoni, S. Leonardi and A. Zare, *Stochastic dynamical wake-modeling for wind farms*, Wind Energy, 2022. Note: Submitted; also arXiv:2208.12196.
- M. Rodrigues, N. Burgess, A. H. Bhatt, S. Leonardi and A. Zare, *Robustness of two-dimensional stochastic dynamical wake models for yawed wind turbines*, In Proceedings of the 2023 American Control Conference, San Diego, CA, 2023. Note: Submitted.
- M. Rodrigues, A. H. Bhatt, F. Bernardoni, S. Leonardi and A. Zare, *Stochastic dynamical modeling of wind farm turbulence*, in Bulletin of the American Physical Society, Indianapolis, IN, 2022.
- A. H. Bhatt, F. Bernardoni, S. Leonardi, and A. Zare, *Stochastic dynamical wake modeling using partially available field measurements*, In Proceedings of the 2022 NAWEA/WindTech Conference, University of Delaware, DE, 2022.
- A. H. Bhatt and A. Zare, *Toward stochastic dynamical wake-modeling for wind farms*, In Proceedings of the 2022 American Control Conference, Atlanta, GA, pp.5241-5246, 2022.

## LEADERSHIP & ORGANISATIONS

---

### Committee Member

*Center of Students and Scholars in Control*

**Mar 2021 — Present**

*Dallas, TX*

- Involved in organising professional and academic events as well as serving as an editor for monthly newsletter for the center.

### Technical Head (Vehicle Dynamics)

*DJS Racing - Formula SAE*

**Sept 2018 — Aug 2019**

*Mumbai, IN*

- Carried out design and analysis of Suspension Kinematics.
- Optimized the wheel hub weight and dimension through CAD modeling and FEA analysis.
- Successfully completed and implemented Tire and Vehicle Models in MATLAB for designing and analysis.
- Calibrated the sensors for data collection from on-track testing.
- Analysed vehicle powertrain and suspension data from on track testing of car to make set-up changes.
- Made executive decisions and handled issues related to car during on-track testing.
- Mentored a group of 30 junior members on concepts related to Vehicle Dynamics.

## PROFESSIONAL ACTIVITIES & APPOINTMENTS

---

- Session chair - *The Bluebonnet Symposium on Thermal-Fluid Sciences*
- Teaching Assistant - Kinematics and Dynamics Laboratory
- Teaching Assistant - Senior Design I & II

**Apr 2022**

**Aug 2021 - May 2022**

**July 2022 - Dec 2022**

## RESEARCH INTEREST

---

- System Modeling and simulation
- Multibody dynamics modeling and analysis
- Control of physical systems
- Convex Optimization
- Application areas - Vehicle controls, transportation technology, sustainable energy

## WORK EXPERIENCE

---

### Motorsport Intern

*JA Motorsports*

**Sep 2019 — Oct 2019**

*Coimbatore, IN*

- Assembled 20 cars for MRF 1600 and Formula 2000.
- Adjusted set-up of race cars on the basis of suspension and aerodynamic parameters.